Nonlinear radiation trapping in an atomic vapor excited by a strong laser pulse

N. N. Bezuglov and A. N. Klucharev
Physics Institute, St. Petersburg University, Ulianovskaya 1, 198904 St. Petersburg, Russia

A. F. Molisch
Institut für Nachrichtentechnik und Hochfrequenztechnik, Technische Universität Wien, Gusshaustrasse 25/389, A-1040 Wien, Austria

M. Allegrini* and F. Fuso
Istituto Nazionale per la Fisica della Materia, Dipartimento di Fisica, Università di Pisa, Piazza Torricelli, 2, I-56100 Pisa, Italy

T. Stacewicz
Institute of Experimental Physics, Warsaw University, Hoza 69, 00-681 Warsaw, Poland
(Received 6 June 1996)

We investigate radiation trapping in an atomic vapor which has been excited by a strong short laser pulse. Since the saturation of the vapor by the pulse leads to a decrease in the effective absorption coefficient, the radiation trapping becomes nonlinear. We derive approximate *analytical* expressions for the excited-state density in the directly excited region, the fluorescence-excited region, and the density averaged over the whole cell. Starting out from fairly simple approximate expressions based on a prescribed distribution of excited atoms, we then develop physically motivated correction factors that drastically improve the accuracy. All these expressions are given for three important cell geometries: the plane-parallel slab, the infinite cylinder, and the sphere. We compare our results to accurate numerical solutions, and find agreement within 5–10%. We then derive the decay time of the emergent radiation, and find that it can be smaller than the natural lifetime of the excited atoms, in agreement with recent experimental results obtained for sodium vapors. [S1063-651X(97)00202-X]

PACS number(s): 51.70.+f, 95.30.Qd, 32.80.Pj, 32.50.+d

I. INTRODUCTION

When an excited-state atom decays to the ground-state, it emits a resonance photon. Such a photon can be absorbed by another ground-state atom, leading to the creation of another excited-state atom. In an atomic vapor cell, this absorption and reemission can be repeated many times until the photon escapes from the cell. The process is known as ''radiation trapping'' [1]. Obviously, it depends strongly on the absorption coefficient of the atoms in the vapor. It is of great interest in chemical physics [2], and has been studied extensively for more than 70 years. Most of the investigations assumed a weak excitation of the vapor, e.g., by collisions with electrons, or radiation from discharge lamps (see, e.g., [3–7]). The distribution of excited-state atoms can be computed from an integrodifferential equation, the so-called Holstein equation (also known as the Biberman-Holstein equation). Under the assumption of weak excitation, it is a *linear* equation.

When an atomic vapor is excited by a very strong laser beam tuned to a resonance transition, the vapor becomes saturated; i.e., the ratio of ground-state atoms and excited-state atoms becomes equal to the ratio of the statistical weights of these levels. This means also that the stimulated emission becomes equal to the absorption, so that the ''effective'' absorption becomes zero, obviously leading to a vanishing of the radiation trapping effects.

One situation that is of particular interest to experiments in chemical and photoplasma physics is the following: we excite part of the vapor cell by a very strong, short laser pulse. Subsequently, we observe the excited-state distribution and the emergent radiation. As time passes, more and more atoms will decay to the ground state by natural decay, so that the effective absorption coefficient increases. However, some of the fluorescence photons are reabsorbed, which diminishes the increase in the effective absorption coefficient. This interrelation causes a strong nonlinearity in the Holstein equation.

Investigation of the nonlinear Holstein equation is a relatively new field. While the effects of saturation on radiation trapping in steady-state vapors and plasmas have been studied for 30 years because of their importance in astrophysics ([8] and references therein), nonlinear time-decay phenomena have received attention only recently, due to the widespread use of powerful pulsed lasers. Previous investigations of this problem have used purely numerical methods: Monte Carlo simulations [9,10], numerical solutions of the equation of radiative transfer, coupled with rate equations [11], or finite-difference solutions of the Holstein equation [12,13]. These methods require, however, a large amount of CPU time, which makes it difficult to study the influence of various parameters by making repeated simulations. An analytical solution of the problem would thus be desirable. In a recent communication [14], we have outlined an approximate analytical computation of the excited-state distribution

*Also at Dipartimento di Fisica della Materia e Tecnologie Fisiche Avanzate, Università di Messina, Salita Sperone 31, I-98166 Sant'Agata, Italy.

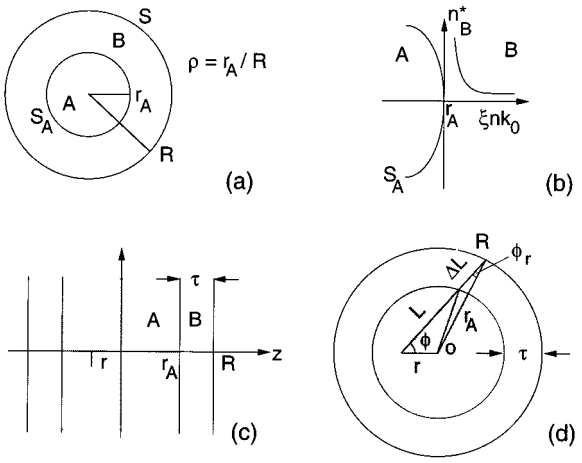

FIG. 1. Sketch of the typical situation for the laser excitation of a gas medium (a), of the geometry relevant for the determination of $N_A^*(t)$ (b), of the slab (c), and cylinder geometries (d) discussed in the text. Region A is directly excited by the laser pulse; parameter ρ gives the relative size of the laser beam.

averaged over the cell. In this paper, we derive a somewhat related method that gives also information on the *spatial* distribution of the excited-state atoms, and we derive physically motivated correction factors that drastically increase the accuracy of the computations. Comparisons with numerical results show the accuracy to be usually better than 5%.

In particular, it is demonstrated that the method of reduced optical depth, which up to now has been employed for plane-parallel geometries only (see, for example, [15]) may be extended with some corrections to describe nonlinear trapping decay problems for curvilinear geometries (cylindrical and spherical). We will also demonstrate that the radiation emerging from the vapor can decay faster than with the natural lifetime of the atoms.

This work is organized as follows: in Sec. II, we define the problem, specify the physical assumptions of the model, and derive the mathematical description. In Secs. III and IV, we derive an approximate analytical solution for the excited-state density averaged over the whole cell, and over the initially excited region, respectively. Section V derives correction factors for these distributions that greatly enhance the accuracy of the method. Section VI discusses the phenomena of a fast (subnatural) decrease of photon flux emerging from the slab, and compares the computed results with data of an experiment performed on sodium vapors. Appendices A through E present details of the mathemical treatments used in our calculations.

II. FORMULATION OF THE PROBLEM

We consider the following situation: a laser illuminates a part (region A, with boundary S_A) of an atomic vapor cell; see Fig. 1(a) [see also Fig. 1(c), where the cell has the shape of a large flat slab]. The aim of our computation is to find the excited-state distribution $n^*(x,t)$; i.e., we want both spatial and temporal information (x denotes the three-dimensional position vector) on the excited state density. For the computations, we make the following assumptions: (i) only two levels in the atomic structure are relevant for the trapping process (e.g. the ground state and first resonance state of an alkali-metal atom); (ii) the walls of the vapor cell are completely transparent; i.e., photons that reach the walls escape from the cell, and are not reflected back into the vapor; (iii) the flight time of the photons is much smaller than the natural lifetime of the excited atoms; (iv) particle diffusion is negligible; (v) collisional quenching and branching (i.e., loss of excitation when atoms decay to the ground state through some intermediate, untrapped transition) is neglected (this assumption will be discussed in more detail in Sec. III); (vi) the emission frequency of a spontaneously emitted photon is independent of the frequency of the previously absorbed photon [complete frequency redistribution (CFR)], and the direction is isotropic; (vii) the geometry of the vapor cell can be approximated as ''one dimensional'' (a plane-parallel slab, an infinitely long cylinder, a sphere), and the initial excitation depends only on one spatial coordinate r which determines (a) the distance from the center plane of the layer, (b) the radial cylinder coordinate and (c) the distance from the sphere center. This also implies that there is no tight focusing of the laser beam, since this would give rise to two-dimensional (2D) effects.

These assumptions are also usually made for the computation of *linear* radiation trapping; they are often fulfilled in laboratory situations (for a discussion, see, e.g., [7]). Furthermore, we assume that (viii) the duration of the exciting laser pulse is much shorter than the natural lifetime of the atoms; (ix) the laser pulse is strong enough to cause appreciable saturation in region A. For example, in sodium atoms, which is the most investigated case [13,16], this requires intensities larger than about 3 kW/cm^2. On the other hand, the intensity must be low enough that high-field effects such as Autler-Townes (ac-Stark splitting) effects are negligible. For the validity of the Holstein theory, the presence of Rabi sidebands must be ignored. In other words, Rabi sidebands must be overlapped within the laser line. Considering typical pulsed laser bandwidths (approximately 0.01 nm), this poses an upper limit to the laser intensity, which must be smaller than ≈ 5 MW/cm^2 [17]. In that range of intensities, multiphoton ionization is also negligible [18,19]. Due to the short duration of the laser pulse (few nanoseconds) and the considered intensity range, the generation of nonthermal electrons during the pump phase (i.e., while the laser pulse is on) is low.

These conditions describe a vapor that is ''softly'' excited by the laser; they are not valid for experiments with exploding targets, where movement of atoms plays an important role; those experiments are beyond the purview of this paper. We are concentrating on a vapor in a sealed cell, where the short laser pulse leads only to an excitation of a bound state (typically the lowest resonance state). The LIBORS (light ionization based on resonance saturation) theory predicts that even under these conditions, practically 10% ionization can occur during the decay phase of initial gas medium excitation [20,21].

In our conditions, both the rate equations and light-vapor interaction are treated within the frame of conventional Biberman-Holstein theory. We start out by defining mathematically the effective spectral absorption coefficient $k(\nu,n^*)$, which describes the difference between absorption and stimulated emission. It depends thus on the ground-state

and excited-state densities, n_1 and n^*, respectively, which in turn depend on spatial coordinate x and time t:

$$k(\nu,x)=k_0\theta_\nu n_1(x,t)\left[1-\frac{n^*(x,t)}{n_1(x,t)}\frac{g_1}{g^*}\right], \tag{1}$$

where g_1 and g^* are the statistical weights of the ground and of the excited state, respectively, k_0 is the absorption coefficient per unit atom in the center of the absorption line, ν_0, and the line shape θ_ν satisfies $\theta_{\nu=\nu_0}=1$.

The opacity χ between two points $x,\tilde{x}$, separated by a distance $\rho=|x-\tilde{x}|$ is given by the integral

$$\chi(\nu,x,\tilde{x};n^*)=\int_x^{\tilde{x}}k(\nu,x_l)dl \tag{2}$$

over a straight line x_l connecting $\tilde{x}$ with x.

The probability G that a photon emitted at $\tilde{x}$ is reabsorbed at x depends on k according to [3]

$$G(x,\tilde{x};n^*)=\frac{1}{4\pi\rho^2}\frac{1}{\int k(\nu,\tilde{x})d\nu}\int k(\nu,x)k(\nu,\tilde{x}) \times\exp[-\chi(\nu,x,\tilde{x};n^*)]d\nu. \tag{3}$$

The excited-state density is decreased by natural decay with the radiation rate constant Γ and it is increased by reabsorption of photons that are emitted somewhere else in the vapor. It is thus described by the following Holstein equation:

$$\frac{\partial n^*(x,t)}{\partial t}=-\Gamma n^*(x,t)+\Gamma\int G(x,\tilde{x};n^*)n^*(\tilde{x},t)d^3\tilde{x}. \tag{4}$$

We see that the reabsorption probability G is the kernel of the (nonlinear) integro-differential equation. The nonlinear behavior occurs due to the dependence of the absorption coefficient k on n^* [Eq. (1)].

The initial condition is given by the assumption of complete saturation in zone A at the end of the pulse ($t=0$): the excited atom density n_A^* becomes a fraction of the atom total density, $n=n^*+n_1$:

$$n_A^*=n_S^*=n\frac{g^*}{g_1+g^*}. \tag{5}$$

Thus, according to Eq. (1), the absorption by the gas medium vanishes, and $k(\nu,n_S^*)=0$ in the region A. We assume that the region A is always in the center of the vessel; its size [radius r_A, see Fig. 1(a)] can be conveniently expressed in R units by introducing the parameter $\rho=r_A/R$.

The behavior of the line shape θ_ν in the wings of the line determines the trapping in an optically dense medium. According to the quasistatic theory of the spectral line broadening, the decrease of θ_ν in the wings is ruled by a power-law function [5,15]

$$\theta_\nu\sim|\nu-\nu_0|^{-\mu}. \tag{6}$$

Formally, the exponential dependence of the Doppler profile can be recovered by placing $\mu=\mu_D=\infty$ in Eq. (6).

III. TOTAL EXCITED-STATE DENSITY

A. Derivation of closed-form equations

In a recent paper [14], we derived a method for the computation of the total number $N^*(t)$ of excited atoms. We first integrate Eq. (4) over the entire volume V of the cell:

$$\frac{dN^*(t)}{dt}=-\Gamma\int_V d^3\tilde{x}n^*(\tilde{x},t)\left[1-\int_V d^3xG(x,\tilde{x};n^*)\right],$$

$$N^*=\int_V n^*(x,t)d^3x. \tag{7}$$

The expression in brackets in Eq. (7) represents the local escape factor $\vartheta(\tilde{x})$, i.e., the probability that a photon emitted at the point $\tilde{x}$ escapes from the vapor cell without being reabsorbed [22,23]. This interpretation is valid for arbitrary spatial distribution of the absorption coefficient [24].

Thus, Eq. (7) can be rewritten as a rate equation:

$$\frac{dN^*}{dt}=-\Gamma N^*\vartheta_{\rm ef}(\tau(N^*)), \tag{8}$$

where $\vartheta_{\rm ef}$ is a spatially averaged value of $\vartheta(x)$, weighted by the spatial distribution of excited-state atoms $n^*(x,t)$:

$$\vartheta_{\rm ef}=\frac{\int_V n^*(x,t)\vartheta(x)d^3x}{\int_V n^*(x,t)d^3x}. \tag{9}$$

We next introduce the ''optical depth'' τ of the vessel, which describes the current opacity of the whole vessel measured along the z axis (for the slab) $\tau=\chi(\nu_0,x_\tau,\tilde{x}_\tau,n^*)$, where $x_\tau=(0,0,0)$ and $\tilde{x}_\tau=(0,0,R)$ [see Fig. 1(c)], or measured along the radial coordinate r (for a cylinder or sphere). The following relationship between τ and N^* is of great importance:

$$\tau(N^*)=\tau^{(M)}\left[1-\frac{N^*(t)}{N_S^*}\right]. \tag{10}$$

In Eq. (10), $N_S^*=Vn_S^*$ is the maximum possible number of excited atoms, corresponding to the entire excitation of the gas volume V, and $\tau^{(M)}=nk_0R$ is the opacity without stimulated emission (i.e., in the linear case).

The transformation to ''optical-depth'' coordinates [using Eq. (10)] is exact [21] for a plane-parallel slab with an arbitrary spatial distribution $n_1^*(x)$. It is also strictly valid, as follows from Eqs. (1) and (2), for uniform $n_1^*(x)$ in cylindrical and spherical geometries, and can be employed approximately for arbitrary $n^*(x)$ in these geometries, as will be discussed below. Due to Eq. (10) the problem of evaluating the escape factor $\vartheta_{\rm ef}$ Eq. (9) may be converted to the case of a spatially homogeneous ground-state (absorbing) atom distribution in a vessel of current opacity τ.

The rate equation for N^* can now be written as

$$\frac{dN^*}{dt} = -\Gamma N^* \vartheta_{\rm ef}\left[\tau^{(M)}\left(1-\frac{N^*}{N_S^*}\right)\right]. \tag{11}$$

In order to evaluate this equation, we need the effective escape factor $\vartheta_{\rm ef}$, which in turn depends on the spatial distribution of excited atoms (i.e., what we want to compute). We circumvent this problem by *assuming* a certain spatial distribution n^* in Eq. (9), namely the fundamental linear mode distribution $n_f(x)$, which is the spatial distribution that occurs for $t\to\infty$ [5,7]. $n_f(x)$ can be expressed through the following analytical approximate expression [5,15]:

$$n_f(r) = \left(1-\frac{r^2}{R^2}\right)^{\gamma}, \tag{12}$$

where the spectral parameter $\gamma=(\mu-1)/2\mu$ is determined by the wings of the line shape as given by Eq. (6). For all possible profiles with $0<\gamma\leqslant 0.5$, the line has broad wings. For the two most important line shapes, i.e., for Lorentz and Doppler profiles, $\gamma_L=0.25$, $\gamma_D=0.5$, respectively. At earlier times, the actual excited-state distribution can differ from the fundamental-mode distribution. The error introduced by this difference will be analyzed below.

With the assumption of a time-independent spatial distribution in Eq. (9), Eq. (11) becomes a one-dimensional nonlinear equation for the determination of N^*. With the initial condition that the volume V_A is completely saturated $[N^*(t=0)=N_S^* V_A/V]$, we get an implicit equation for N^*, the excited-state density integrated over the whole cell:

$$t\Gamma = \int_{N^*/N_S^*}^{V_A/V} \frac{du}{u}\,\frac{1}{\vartheta_{\rm ef}[\tau^{(M)}(1-u)]} = I\left(\frac{N^*}{N_S}\right) - I\left(\frac{V_A}{V}\right), \tag{13}$$

where

$$I(p) = \int_p^1 \frac{du}{u}\,\frac{1}{\vartheta_{\rm ef}[\tau^{(M)}(1-u)]}. \tag{14}$$

According to the derivation discussed in Appendix B, the integral $I(p)$ has closed-form approximations for both Lorentz and Doppler profiles:

$$I^{(L)}(p) = \frac{1.5}{\vartheta_{\rm ef}^{(L)}[\tau^{(M)}(1-p)/2.25]} \times\left[\frac{1}{\sqrt{1-p}}\ln\frac{1+\sqrt{1-p}}{1-1\sqrt{1-p}}-2\right], \tag{15}$$

$$I^{(D)}(p) = \frac{2}{\vartheta_{\rm ef}^{(D)}[\tau^{(M)}(1-p)/2]}\left[\frac{-\ln(p)}{1-p}-1\right]. \tag{16}$$

Thus, these equations provide an analytical solution for one important parameter of the vapor, the total number of excited-state atoms.

If also quenching or branching occur, then we would have to add a term $[-(\Gamma_b+Q)N^*]$ on the right-hand side of Eq. (8), where Γ_b is the radiative decay rate of the untrapped transitions emanating from the excited state, and Q is the quenching rate for collisional quenching. This term modifies also Eq. (13) by the following replacement: $\vartheta_{\rm ef}$ is changed by $\vartheta_{\rm ef}[\tau^{(M)}(1-u)]+(\Gamma_b+Q)/\Gamma$.

This shows that a rather straightforward inclusion of branching and quenching is possible. However, for the analysis of the lowest resonance state of sodium atoms treated explicitly in the present work, these effects can be neglected. Branching cannot occur, since there are no intermediate levels between the excited and the ground state. For self-quenching, we can compute the typical rates as the product of the density ($10^{13}-10^{14}$ cm^{-3}), the self-quenching cross section (10^{-14} cm^2), and the velocity (10^4 cm/s). Quenching effects occur thus on a time scale of 10^{-4} s, which is much larger than the observation time, typically less than 10^{-6} s. If a noble gas is present in the cell, then the foreign-gas quenching is of the same order as the self-quenching: while the densities for the noble gas are much higher, the quenching cross sections are much lower. For other experimental situations, however, quenching or branching might be relevant.

The situation becomes even more complicated if there is very strong hyperfine splitting (hfs) of the ground state, as occurs in rubidium and cesium. In these atoms, the splitting is so strong that the hf levels must be regarded as distinct levels that are all appreciably populated, so that the transitions from the excited state to hfs levels are all trapped. In that case, we have to set up a system of equations similar to Eq. (8), but with the escape factor depending on the densities in all states. To our knowledge, a closed-form solution of the type of Eq. (13) is not yet available for that kind of problem. Furthermore, new physical effects, such as optical pumping [25], can occur in these configurations. Numerical solutions of this problem have been given in [26].

Nevertheless the two-level model works nicely in the case of alkali atoms such as sodium. If the linewidth of the laser is large, one can consider the resonance saturation of the $3S_{1/2}\to 3P_{1/2}$ (or $3S_{1/2}\to 3P_{3/2}$) transition to lead to an equal population of all hf sublevels. During the decay phase, the large Doppler or Lorentz linewidth covers all hyperfine effects [27].

In the remainder of the paper, we will confine our attention to the canonical case of a true two-level atom without quenching or branching.

B. Computation of the escape factor

We now take a look at the escape factor for various spatial distributions, and investigate the error introduced by the assumption of a time-invariant spatial distribution. As mentioned above, the assumed distribution n_f is close to the actual one at late times, but not necessarily at early times. The largest differences will occur if V_A is very small [in that case, the $n^*(x,0)$ approximates a δ distribution at the center of the cell), or if $V_A=V$ [in that case $n^*(x,0)$ is uniform]. In order to find the maximum error introduced by this difference, we now examine the escape factors [Eq. (9)] for a broad class of power-law distribution functions $n^*(x,t)=n_m(r)$:

$$n_m(r) = \left(1-\frac{r^2}{R^2}\right)^m, \quad 0\leqslant m<\infty. \tag{17}$$

For a power index $m=0$, $n_0(r)$ describes a spatially uniform

TABLE I. Escape factors for different geometries and line profiles.

		Layer $\kappa=1$	Cylinder $\kappa=2$	Sphere $\kappa=3$
Doppler profile Q_D	$\delta(m=\infty)$	$\frac{1}{2}$	$\frac{\pi}{4}$	1
	fundamental mode	0.91	1.58	2.14
	$m=0.5$	1	$\frac{3\pi^2}{16}\simeq 1.85$	$\frac{8}{3}\simeq 2.67$
	$m=0$	$\frac{\ln\tau}{2}$	$\ln\tau$	$\frac{3}{2}\ln\tau$
Lorentz profile Q_L	$\delta(m=\infty)$	$\frac{2}{3}$	$\frac{2\sqrt{\pi}\Gamma(1.25)}{3\Gamma(0.75)}\simeq 0.87$	1
	fundamental mode	0.81	1.12	1.34
	$m=0.5$	$\frac{16\sqrt{2}}{9\pi}\simeq 0.80$	$\frac{8}{5\sqrt{2}}\simeq 1.13$	$\frac{16\cdot 8}{21\pi\sqrt{2}}\simeq 1.37$
	$m=0$	$\frac{2\sqrt{2}}{3}\simeq 0.94$	$\frac{8\pi}{9}\frac{\Gamma(1.25)}{\Gamma^3(0.75)}\simeq 1.37$	$\frac{6\sqrt{2}}{5}\simeq 1.69$

distribution. For large m values, it is possible to write a series expansion of Eq. (17) for $r\sim 0$: $(1-r^2/R^2)^m\simeq \exp(-mr^2/R^2)$. Thus, $m\to\infty$ corresponds to a sharp localization in the cell center (the radiation constant $1/\vartheta_{\rm ef}^{(\delta)}$ is known in this case as Biberman's effective lifetime [4,22]): $n_\infty(r)=\delta(r)$. When $m=\gamma$, Eq. (17) describes obviously the fundamental mode $n_f(r)$ [Eq. (12)].

Thus the functions $n_m(r)$ introduced by Eq. (17) cover all space distributions $n^*(r,t)$ occurring while the decay process takes place.

In Appendix A we derive a general formula for the asymptotic behavior ($\tau=k_0nR\to\infty$) of the escape factor, which is valid for all the three geometries considered in this work:

$$\vartheta_{\rm ef}^{(m)}(\tau)=T(\tau)\frac{\sqrt{\pi}\ \ \Gamma(\kappa/2+\gamma)}{2\Gamma(1.5+\gamma)\Gamma(\kappa/2)}\times\left[\frac{\Gamma(1+m-2\gamma)\Gamma(\kappa/2+m+1)}{\Gamma(1+m-\gamma)\Gamma(\kappa/2+m+1-\gamma)}\right], \quad (18)$$

where $\Gamma(\Phi)$ is the Euler Γ function with argument Φ. The parameter κ entering Eq. (18) describes the type of geometry: $\kappa=1$ for a plane-parallel slab of total thickness $2R$; $\kappa=2$ for a cylinder with radius R; $\kappa=3$ for a sphere with radius R. The function $T(\tau)$ in Eq. (18) gives the transmission factor through a layer of opacity τ [15,23]:

$$T(\tau)=\int \varphi_\nu\exp(-\tau\theta_\nu)d\nu, \quad \varphi_\nu=\frac{k_\nu}{\int k_\nu d\nu} \quad (19)$$

with the well-known properties [15]

$$T(\tau)\underset{\tau\to 1}{\simeq} 1, \quad T(\tau)\underset{\tau\to\infty}{\simeq}\frac{c}{\tau^{2\gamma}}, \quad T(\tau z)\underset{\tau\to\infty}{\simeq}\frac{T(\tau)}{z^{2\gamma}}. \quad (20)$$

According to Eq. (18), the same factorization properties as those given in the last equation of Eq. (20) are valid also for the escape factor $\vartheta_{\rm ef}^{(m)}(\tau z)$. This fact will be used extensively in the following. Note that the expression in brackets in Eq. (18) becomes equal to unity when $m\to\infty$. It implies that the part of Eq. (18) not enclosed in brackets gives the $\vartheta_{\rm ef}^{(\delta)}$ factor.

For Doppler and Lorentz spectral profiles, Eq. (18) can be written as follows:

$$\text{Doppler:} \quad \vartheta_{\rm ef}^{(m)}(\tau)=\frac{Q_D^{(m)}}{\tau\sqrt{\pi\ln(\tau)}}, \quad T^{(D)}(\tau)\sim\frac{1}{\tau\sqrt{\pi\ln(\tau)}}, \quad (21)$$

$$\text{Lorentz:} \quad \vartheta_{\rm ef}^{(m)}(\tau)=\frac{Q_L^{(m)}}{\sqrt{\pi\tau}}, \quad T^{(L)}(\tau)\sim\frac{1}{\sqrt{\pi\tau}}. \quad (22)$$

The values of $Q_D^{(m)}$ and $Q_L^{(m)}$ parameters are presented in Table I for the three geometries considered in this paper. In the table, the escape factors of the ground (Holstein) mode $\vartheta_{\rm ef}^{(H)}\simeq Q_\gamma^{(H)}T(\tau)$ are also reported [7]. Note that $\Gamma(1+m-2\gamma)=\Gamma(1-2\gamma)\to\infty$ when $m=0$ for Doppler profile ($\gamma=0.5$). This divergence is the reason [28] for the appearance of the function $\ln(\tau)$ in Table I.

Equation (18) is not valid in the low-opacity region $\tau\leqslant 5$. An expression suitable for the evaluation of $\vartheta_{\rm ef}^{(m)}$ is derived in Appendix A (see also [28]):

$$\vartheta_{\rm ef}^{(m)}(\tau)=\frac{\Gamma(\kappa/2+m+1)}{\Gamma(\kappa/2)}2^{1+m}\int_0^\infty d\nu\varphi_\nu\tau\theta_\nu\int_{\tau\theta_\nu}^\infty\frac{dz}{z^{m+2}}$$
$$\times I_{\kappa/2+m}(z)K_{\kappa/2}(z), \tag{23}$$

where I_λ and K_λ are modified Bessel functions of the first and second kind [29]. In the case that the excited atoms are concentrated in the center of the cell ($m=\infty$), Eq. (23) immediately reduces to

$$\vartheta_{\rm ef}^{(\delta)}(\tau)=\frac{2^{1-\kappa/2}}{\Gamma(\kappa/2)}\int_0^\infty d\nu\varphi_\nu\tau\theta_\nu\int_{\tau\theta_\nu}^\infty dz z^{\kappa/2-2}K_{\kappa/2}(z). \tag{24}$$

Note that, for all m values, $\vartheta_{\rm ef}^{(m)}(\tau)\simeq 1$ for $\tau\sim 0$. This is in agreement with a general consideration: photons escape the gas medium freely for small opacities.

The comparison between different $Q^{(m)}$ values (see Table I) points out that for a Doppler profile, when $\tau\gg 1$, the escape factors strongly depend on the spatial distribution of n^*: for a uniform distribution ($m=0$), Q_D contains a factor $\ln(\tau)$, which can become very large at large opacities. For other distributions, however, the $Q^{(m)}$ values are constants.

IV. DETERMINATION OF $N_A^*(T)$ IN THE VOLUME A

In this section, we derive a closed-form equation for $n_A^*(t)$, the excited-state density in the directly excited region A. We consider only early times; we know that at late times, the problem is linear and the spatial distribution is actually described by the fundamental mode. We can thus make the following two simplifications: (i) within the volume V_A, the density n^* remains practically uniform, so the total number N_A^* of the excited atoms in V_A is $n_A^*V_A$; this assumption will be fulfilled longer for a smaller ratio V_A/V; (ii) the secondary excited atoms in the region B are localized mainly close to the surface S_A [see Fig. 1(b)]; excitation of atoms in the region B is due to the photons emerging from region A. This assumption is actually not fulfilled for a low-opacity vapor. However, we will see that the results of our derivation agree well with the numerical calculations already for opacities $\tau=2$ (see Fig. 3), and radiation trapping effects in vapors with even lower opacities are small anyway.

In the early stage of the decay, the optical thickness of region A remains small and the spectrum of the radiation emerging from region A is not affected by self-reversal. In this case, the dominant source of excitation in region B has a space behavior ruled by a power-law, with $dT(\xi)/d\xi$ decreasing as $(\xi nk_0)^{-1-2\gamma}$, where ξ denotes a coordinate in the region B along the direction normal to S_A. For large opacities, this distribution corresponds to a δ distribution near the surface S_A of region A [see Fig. 1(b)].

Since by assumption $n_A^*(x,t)$ is independent of x, it is sufficient to consider the case $x=0$. Equation (4) can then be written as (for the sake of simplicity, we henceforth omit the argument n^* from the kernel G)

$$\left.\frac{dn_A^*}{dt}\right|_{r=0}=-n_A^*(r=0,t)\Gamma\left[1-\int_{V_A}d^3\tilde{x}G(r=0,\tilde{x})\right]$$
$$+\Gamma\int_{V_B}G(0,\tilde{x})n^*(\tilde{x},t)d^3\tilde{x}. \tag{25}$$

The first term in brackets on the right-hand side is the escape factor from region A, similar to that introduced in Eq. (7) (i.e., the probability of escaping from the center of region A without being reabsorbed). Since we have already made an assumption about the spatial distribution of excited-state atoms, the evaluation is straightforward:

$$1-\int_{V_A}G(r=0,\tilde{x})d\tilde{x}=\vartheta_{\rm ef}^{m=\infty}(\tau_A^*(t)), \tag{26}$$

with

$$\tau_A^*(t)=\tau_A^{(M)}\left(1-\frac{n_A^*}{n_S^*}\right), \tag{27}$$

where $\tau_A^{(M)}=k_0nr_A$ is the maximum linear opacity for the directly excited region A [compare with Eq. (10)].

For the evaluation of the second term in Eq. (25), we use the fact that n_B^* is concentrated near the boundary between region A and region B. Thus, integration over V_B can be restricted to a small volume V_Δ close to S_A:

$$\int_{V_B}d^3\tilde{x}G(0,\tilde{x})n^*(\tilde{x},t)\underset{V_\Delta\to 0}{=}\int_{V_B}n^*(\tilde{x},t)d^3\tilde{x}\frac{\int_{V_\Delta}d^3\tilde{x}G(0,\tilde{x})}{\int_{V_\Delta}d^3\tilde{x}}. \tag{28}$$

The L'Hopital rule can be used to determine the ratio appearing in Eq. (28):

$$\int_{V_B}d^3\tilde{x}G(0,\tilde{x})n^*=N_B^*(t)\left.\frac{-(d/dr)\vartheta_{\rm ef}^{(\delta)}}{(d/dr)V(r)}\right|_{r=r_A}, \tag{29}$$

where we have introduced the escape factor $\vartheta_{\rm ef}^{(\delta)}$:

$$\vartheta_{\rm ef}^{(\delta)}=1-\int_{V_r}d^3\tilde{x}G(r=0,\tilde{x}), \tag{30}$$

which corresponds to the Biberman escape factor for a volume of radius r. According to the notations introduced just after Eqs. (7) and (17), $\vartheta_{\rm ef}^{(\delta)}$ corresponds to the escape factor with $m=\infty$.

Equation (25) can then be written in the form

$$\frac{dN_A^*(t)}{dt}=-\Gamma\vartheta_{\rm ef}^{(\delta)}\left(\tau_A^{(M)}\left(1-\frac{N_A^*}{n_S^*V_A}\right)\right)N_A^*(t)+\Gamma(N^*-N_A^*)$$
$$\times\vartheta_{\rm ex}\left(\tau_A^{(M)}\left(1-\frac{N_A^*}{n_S^*V_A}\right)\right), \tag{31}$$

where

$$\vartheta_{\rm ex}(x)=-\frac{x}{\kappa}\frac{d\vartheta_{\rm ef}^{(\delta)}(x)}{dx}, \tag{32}$$

and we have introduced the total number of excited atoms in region A, $N_A^* = V_A n_A^*$.

The right-hand side of Eq. (31) consists of two terms. The first one is the rate with which N_A decreases because of the photons leaving region A. The second term corresponds to photons that are emitted in region B (from secondary-excited atoms) and are reabsorbed in region A. Since the explicit dependence of $N^*(t)$ on time t is given by Eqs. (11) and (13), it is possible to derive a one-dimensional closed equation for the determination of $N_A^*(t)$ with the initial condition $N_A^*(t=0) = n_S^* V_A$. In practice, it is more convenient to solve Eq. (31) by exploiting the time dependence of N^* on t:

$$\frac{dN_A^*(t)}{dt} = \frac{dN_A^*}{dN^*}\frac{dN^*}{dt} = -\Gamma N^* \vartheta_{\rm ef}^{(m)}\left(\tau^{(M)}\left(1-\frac{N^*}{N_S^*}\right)\right)\frac{dN_A^*}{dN^*}, \tag{33}$$

This allows us to treat N_A^* as a function of N^* in Eq. (31).

Before discussing the results of our analysis, we present here some features of the rate constant $\vartheta_{\rm ex}$ that will be useful in the following:

$$\vartheta_{\rm ex}(x) \underset{x\to 0}{\sim} x, \quad \vartheta_{\rm ex}(x) \underset{x\to\infty}{\sim} 2\gamma Q^{(\delta)} T(x)/\kappa. \tag{34}$$

In addition, according to the definition given in Eq. (32), the following expression for $\vartheta_{\rm ex}$ can be derived from Eq. (24):

$$\vartheta_{\rm ex}(\tau) = \frac{2^{1-\kappa/2}}{\kappa\Gamma(\kappa/2)}\int_0^\infty d\nu \varphi_\nu \tau\theta_\nu \int_{\tau\theta_\nu}^\infty dz z^{\kappa/2-1} K_{\kappa/2-1}(z). \tag{35}$$

The behavior of $\vartheta_{\rm ex}$ as a function of x stated in Eq. (34) for small x follows directly from Eq. (35), whereas the asymptotic behavior for $x\to\infty$ is determined by Eqs. (18)–(22).

Figure 2 shows the excited-state density in a slab with $\tau = 10$. Numerical solutions are shown as solid curves, and the analytical solutions N^*, N_A^* of Eqs. (11) and (31) (with $\vartheta_{\rm ef} = \vartheta_{\rm ef}^{(m=0.5)}$) are represented with dotted lines. We see that the agreement for N^* is quite good, as anticipated from Ref. [14]. However, the solutions for N_A^*, N_B^* show considerable deviations, so that additional analysis is required to improve our solutions.

V. CORRECTION FACTORS

In the previous sections, we have derived analytical equations, Eqs. (11) and (31), which explain the main features of the nonlinear decay process. In order to derive this description, we have introduced three basic assumptions: (i) the spatial distribution of excited atoms in Eq. (9) is always identical to the lowest-order mode distribution; (ii) the connection between the current opacity $\tau(t)$ and $N^*(t)$ [Eq. (10)], which is valid strictly for a plane-parallel slab, can be used for curvilinear geometries; (iii) all atoms in region B are concentrated near the boundary between regions A and B. In this section, we will analyze these three assumptions and compute the maximum error caused by them. More importantly, we will derive physically motivated correction factors, which greatly increase the accuracy of the description.

The main idea for the correction factors is the analysis of the excited-state distribution for two crucial limiting cases: (i) at the beginning of the decay, when the equations have a nonlinear behavior because of the saturation of the gas medium by the laser pulse; (ii) in the final stage of the decay (linear part), which is ruled only by the fundamental mode space distribution n_f^*, with an effective lifetime $1/(\Gamma\vartheta_{\rm ef}^{(H)})$. These limiting cases can be investigated analytically by various methods; the correct behavior of the solutions of Eqs. (11) and (31) is then enforced by modifying the rate constants in these equations. If we can get a correct description at early and late times, we can anticipate that this description will also work well at intermediate times, as is confirmed by comparisons with numerical simulations.

We can see from Table I that for a Doppler line shape the escape factor depends strongly on the excited-state distribution, while this dependence is much weaker for the Lorentz profile. The Doppler shape thus represents the most difficult situation and will be at the center of our attention in this section; the results are also valid for the Lorentz profile.

A. Corrections to the one-mode approach

The first and most important assumption is that the excited-state distribution does not vary with time; we call this the one-mode approach (although, strictly speaking, there are no modes in a nonlinear problem). At early times, this assumption is not true. The physical processes occurring at early times can best be explained for the slab geometry; here we can replace the spatial coordinate z by an optical depth coordinate τ:

$$\tau(z,t) = k_0 \int_0^z d\tilde{z}\left[n_1(\tilde{z},t) - \frac{g_1}{g^*} n^*(\tilde{z},t)\right], \tag{36}$$

which gives the opacity $\tau(z,t)$ of the slab between the coordinates 0 and z at the instant t. This coordinate transformation allows one to treat problems with an inhomogeneous absorption coefficient in exactly the same way as the well-known problems with homogeneous absorption coefficients.

In the τ space, the equation for $N^*(t)$ has the form [21]

$$\frac{dN^*}{dt} = -\Gamma N^*(t)\frac{1}{\displaystyle\int_{-\tau(t)}^{\tau(t)} d\tilde{\tau} n^*(\tilde{\tau},t)}\int_{-\tau(t)}^{\tau(t)} d\tilde{\tau} n^*(\tilde{\tau},t)\,\vartheta(\tilde{\tau}), \tag{37}$$

where $\vartheta(\tau)$ is exactly the local escape factor for a layer of current total optical opacity $2\tau(t)$. Due to Eq. (36), and to the fact that $n = n_1 + n^*$ is a constant along the space coordinate, we immediately obtain the relationship of Eq. (10), which connects $\tau(t)$ with $N^*(t)$. This reduces the problem of evaluating the rate constant $\vartheta_{\rm ef}$ in Eq. (11) to a homogeneous absorption medium situation.

Let us examine the case where the laser excites the whole vapor cell, $V_A = V$ ($\rho = 1$). Thus, at the first instant, the excitation is uniform, and τ space and z space are equivalent. As time goes on, the decay will be strongest near the cell walls, so that there we will have a larger effective absorption coefficient than in the middle of the cell. This means that the (in geometrical space) small region where we have a larger

TABLE II. Values of the c constant for different geometries.

		Layer $\kappa=1$	Cylinder $\kappa=2$	Sphere $\kappa=3$
Doppler profile c_D	$\rho=0$	$1.27\left(\frac{3\pi}{8}\simeq 1.18\right)$	$1.43(\frac{4}{3}\simeq 1.33)$	$1.57\left(\frac{15\pi^2}{32}\simeq 1.47\right)$
	$\rho=1$	$0.81\left(\frac{3\pi^2}{32}\simeq 0.92\right)$	$0.80(\frac{8}{9}\simeq 0.91)$	0.77(0.87)
Lorentz profile c_L	$\rho=0$	1.11	1.20	1.27
	$\rho=1$	0.97	0.96	0.95

percentage of ground-state atoms transforms into a (in τ space) larger region (in the case $\tau^{(M)}\gg 1$).

This implies in turn that, in the τ space, the distribution of excited-state atoms decays very quickly to the fundamental-mode distribution. Furthermore, the error at early times is very small due to the following fact: The opacity $\tau(t=0)$, which is zero at the beginning of the process, remains small during the evolution of the $n^*_{\rho=1}$ distribution into the fundamental distribution. However, the escape factor $\vartheta^{(m)}_{\rm ef}$ is not sensitive to the actual m values when $\tau(t)$ is small. We have seen in the previous sections that the difference in Q_D between $m=0$ and $m=0.5$ can become very large. However, the above discussion demonstrates that the nonlinearity of the problem actually *decreases* this difference.

If the laser excites only part of the vapor cell, then the initial distribution in τ space is a δ distribution: region A contributes nothing to the opacity, so that all points in this region are at $\tau=0$. As time increases, the fluorescence photons are emitted, and most of them are absorbed near the boundary S_A, leading to a bleaching effect also in this boundary region: $\tau_B(t)<\tau_B(t=0)$. Moreover, there is another change in the τ coordinate: points in region A (but with $z\neq 0$) that were previously at $\tau=0$ are now at some point τ different from zero, i.e., closer to the cell walls. These effects again help to reach the fundamental-mode distribution in a relatively short time.

Finally, if the laser excites only a very small region in the center of the slab, we have no nonlinearity at all; τ space and geometrical space are equivalent. The problem is the same as a linear trapping problem with a δ initial distribution. Being the most difficult situation, it also provides the limits for the accuracy of the one-mode approach.

In Appendix C, we show how the correct behavior at early and late times can be recovered by introducing a time-variant opacity into the solution Eqs. (11) and (31), i.e. by substituting

$$\tau^{(M)}\rightarrow\tau^{(M)}\left(1+\Delta_\rho\frac{N^*(t)}{N^*(t=0)}\right), \tag{38}$$

where

$$\Delta_\rho=(1-\rho^\kappa)(c_{\rho=0}-1) \tag{39}$$

and $c_{\rho=0}$ is given in Table II in the line ''Doppler profile'' (the presence of the numbers in brackets will be explained in Appendix C).

The analysis of Appendix C allows one to estimate the final error in the evaluation of the total number of excited atoms $N^*(t)$ by means of Eqs. (11), (38), and (39) as $\approx 5\%$. This is demonstrated by the N^*-curves of Figs. 2–4, which show N^*, N^*_A, and N^*_B for various opacities ($\tau=2,10$) and intial excitations ($\rho=0.25,0.5$) for Doppler and Lorentz profiles. We see that we get good agreement (error less than 10%) for all cases. We see from the figures that the agreement is better for Lorentz than for Doppler line shapes, in accordance with the results of the qualitative dis-

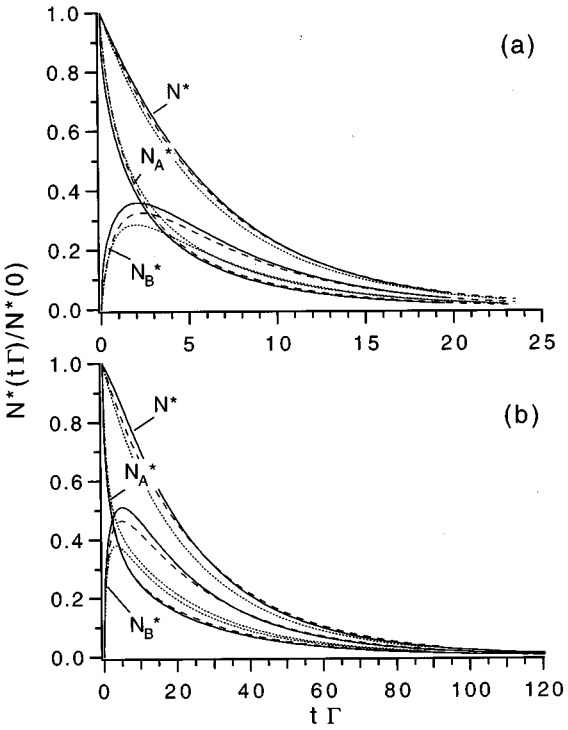

FIG. 2. Slab with $\tau^{(M)}=10$, $\rho=0.25$: normalized decay curves for the total number of excited atoms in all the considered volume (N^*), in region A (N^*_A) and in region B (N^*_B), for Lorentz (a) and Doppler (b) profiles. The solid lines represent the result of the numerical simulations, according to [13]; the dotted lines are the solutions with the analytical equations of Secs. III and IV; the dashed lines are the analytical solutions including the correction factors of Sec. V.

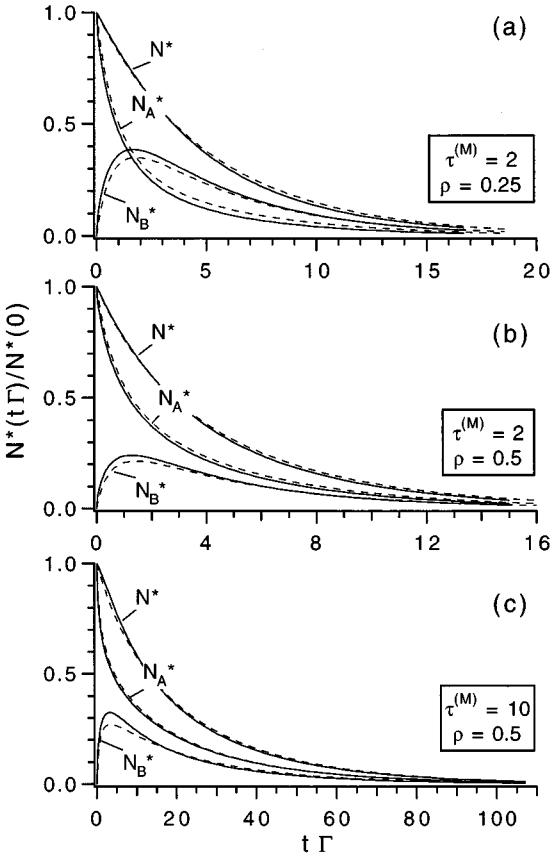

FIG. 3. Partially excited slab with various opacities $\tau^{(M)}=2$ or 10 and various initial excitations ($\rho=0.25$ or 0.5): normalized decay curves for the total number of excited atoms in all the considered volume (N^*), in region A (N_A^*) and in region B (N_B^*) for Doppler profile. The solid and dashed lines represent the results of the numerical and analytical [Eqs. (40)–(43)] simulations, respectively.

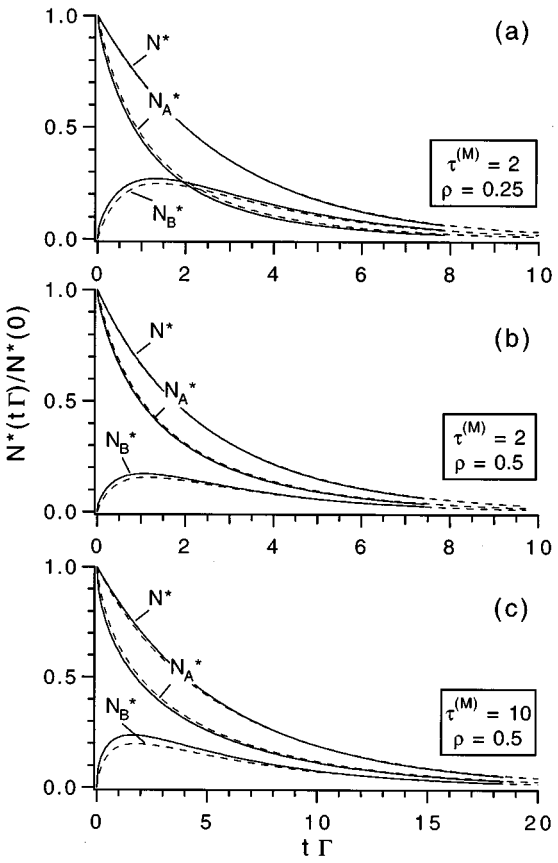

FIG. 4. Same as Fig. 3, but with Lorentzian line shape.

cussion given above. It is thus also clear that the error for a Voigt line will be somewhere between the error for a Doppler line and the error for a Lorentz line; in other words, the error for the Doppler line is the upper limit for all practically occurring line shapes. Further examples of the results found for the entirely excited layer ($\rho=1$) are presented in our previous work [14] (note that the correction factor for the entirely excited slab vanishes).

B. Corrections on the geometry

The computations in the plane-parallel slab are simplified by the fact that we can introduce the optical-density coordinate τ in Eq. (36). In the first moment, the whole region A corresponds to $\tau=0$; i.e., the escape of the photons is independent of the geometrical position z within region A. The local escape factor $\vartheta_L(r)$ is determined essentially by the linear opacity $\tau=k_0 n(R-r_A)$ of the region B [see the sketch shown in Fig. 1(c)]. Assuming Eq (10) to be valid for all types of cells under investigation we thus simulated formally the situations occurring in the linear geometry. For curvilinear geometries (cylindrical, spherical), the above simplification, however, is not possible anymore. This fact can be understood more easily considering a sphere. A photon emitted in the center of the sphere has to cover a geometrical path length r_A through region A (which is transparent), and $R-r_A$ through region B, since the direction of propagation is normal on the surface of the sphere. This is the shortest possible length for escape. However, a photon that is emitted at some other point in region A can have a direction that has some angle with respect to the normal on the surface, so that the path length through region B is larger. Thus, the opacity, and hence the escape factor, depends on the position of the emitting atom. This fact has to be included in the simulations. As shown in Appendix D, the geometry correction can be written by modifying the opacity — exactly as for the single-mode correction. More precisely, we make the substitution $\tau\rightarrow\tau(1+\Delta_G)$, where $\Delta_G=\Delta_C=0.19$ for a cylinder and $\Delta_G=\Delta_S=0.33$ for a sphere in the case $\rho\sim1$. This describes the change in the escape factor (as compared to the usual escape factor in a cylinder or a sphere) that is due to a hollow-cylinder or hollow-sphere geometry. This geometry is valid only at the beginning of the decay process; at later times, we have the normal geometry. The correction must thus be implemented at the beginning, and vanishes at late times; this problem is similar to the single-mode correction described in the previous subsection. We can thus use Eq. (38) for taking into account the geometry correction factors.

There is, however, one important difference: for the single-mode correction, the correction was large when the initially excited region was very small, $\rho=0$, and zero for $\rho=1$. For the geometry modifications, the correction is zero for $\rho=0$ and large for $\rho=1$, so that it is reasonable to approximate it as $\Delta_G(\rho)=\rho^\kappa\Delta_G$ [compare with Eq. (39)]. Thus

TABLE III. Correction factors Δ for different geometries.

	Layer $\kappa=1$	Cylinder $\kappa=2$	Sphere $\kappa=3$
Δ	$0.27\,(1-\rho)$	0.30	0.45
Δ_A	0	0.30	0.45
$\Delta_A^{(\mathrm{ex})}$	0	0.19	0.33

the total correction $\Delta(\kappa=2,3)$, i.e., the sum $\Delta=\Delta_\rho+\Delta_G(\rho)$, is nearly independent of ρ. We will take $\Delta=[\Delta_{\rho=0}+\Delta_G(\rho=1)]/2$, that, as is seen from Table I and Eqs. (D9) and (D10), corresponds to a 10% accuracy in the evaluation of τ for $\kappa=2,3$. Table III shows the values of Δ for the three geometries under investigation.

Let us summarize the results presented in Secs. V A and V B by writing the relevant rate equations with all the corrections included:

$$\frac{dN^*}{dt}=-\Gamma N^*\vartheta_{\mathrm{ef}}^{(m=0.5)}(\tau(t)), \tag{40}$$

$$\tau(t)=\tau^{(M)}\left(1-\frac{N^*(t)}{n_S^*V}\right)\left(1+\Delta\frac{N^*(t)}{n_S^*V_A}\right), \tag{41}$$

$$\frac{dN_A^*(t)}{dt}=-\Gamma\vartheta_{\mathrm{ef}}^{(m=0.5)}(\tau_A(t))N_A^*(t)+\Gamma(N^*-N_A^*) \times\vartheta_{\mathrm{ex}}(\tau_A^{(\mathrm{ex})}(t)\lambda)\lambda^{-1}, \tag{42}$$

$$\tau_A(t)=\tau_A^{(M)}\left(1-\frac{N_A^*(t)}{n_S^*V_A}\right)\left(1+\Delta_A\frac{N_A^*(t)}{n_S^*V_A}\right). \tag{43}$$

The appearance of the factor λ in Eq. (42) will be discussed in the next section.

The geometry correction must also be carried out for region A. The prime excitation of region A corresponds formally to the case $\rho\sim1$. We decided, nevertheless, to use $\Delta_A=\Delta$ in Eq. (43) (see Table III) in order to avoid discrepancies between Eqs. (40) and (42) for $\rho\sim1$ [for the same reason, in Eq. (42) the escape factor $\vartheta_{\mathrm{ef}}^{(m=0.5)}$ is chosen instead of $\vartheta_{\mathrm{ef}}^{(\delta)}$ entering Eq. (31)]. However, the best choice for $\Delta_A^{(\mathrm{ex})}$ is $\Delta_G=\Delta_{S,C}$ as is determined in Appendx D by Eqs. (D9) and (D10).

The effectiveness of the corrections is demonstrated in Fig. 5, which shows the excited-state density in a cylinder with and without the correction factor: the accuracy including the Δ factor is better than 10%, in agreement with the above presented analysis.

C. Corrections on the atom distribution n_B^*

The third assumption in the derivation of Eq. (31) was that the excited-state atoms in region B are concentrated near the boundary S to region A. This assumption is valid at the beginning of the decay, more precisely, during the time interval $0\leqslant t\leqslant T_{\mathrm{inc}}$, while the total excitation in region B is growing. However, it is not valid at late times, where the distribution has the shape of the lowest-order mode.

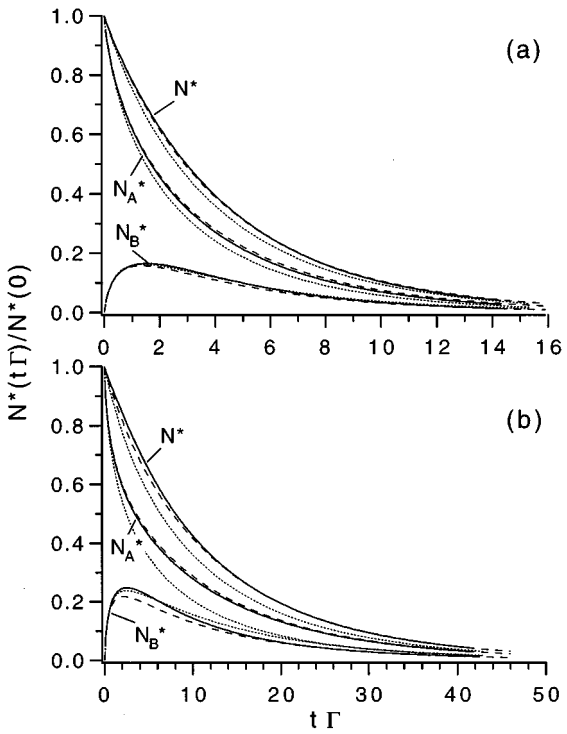

FIG. 5. Cylinder with $\tau^{(M)}=10$, $\rho=0.7$: normalized decay curves for the total number of excited atoms in all the considered volume (N^*), in region A (N_A^*) and in region B (N_B^*), for Lorentz (a) and Doppler (b) profiles. The solid lines represent the result of the numerical simulations, according to [12]; the dotted and dashed lines are the solutions without and with correction factors, respectively .

The basic idea of the correction factor is the following: if the opacity of region A is small (i.e., at the beginning of the decay), the probability that a secondary photon (emitted in region B) is absorbed in region A increases approximately linearly with the opacity τ_A [see Eq. (34)]. If the opacity of region A is large (i.e., at late times), a further increase in the opacity hardly changes the reabsorption probability. If we thus use a correction factor λ so that

$$\vartheta_{\mathrm{ex}}(\tau_A(t))\rightarrow\vartheta_{\mathrm{ex}}(\lambda\tau_A(t))\lambda^{-1}, \tag{44}$$

it does not affect the N_A^* curves at the beginning of the decay $\lambda\tau_A(t)<1$ [see Eq. (34)], when no correction is needed. On the contrary, the λ factor influences strongly the value of ϑ_{ex} for large $\tau_A(t)$. A proper choice of λ thus allows one to account for the space diffusion effects for excited atoms coming from radiation trapping processes in region B.

The derivation for the factor λ is given in Appendix E. For the three geometries under consideration, we obtain

$$\lambda_{\kappa=1}^2=\frac{\pi}{4}\ \frac{1-\rho^2/2}{2\rho}\ \frac{1-\rho(1-8/(3\pi))}{1-\rho^2(1-\pi/4)}\Lambda_{\kappa=1}(\tau_A^{(M)}), \tag{45}$$

$$\lambda_{\kappa=2}^2=\frac{4}{3\pi}\ \frac{1-\rho^2/2}{3\rho^2}\ \frac{1+\rho}{1-\rho^2/3}\Lambda_{\kappa=2}(\tau_A^{(M)}), \tag{46}$$

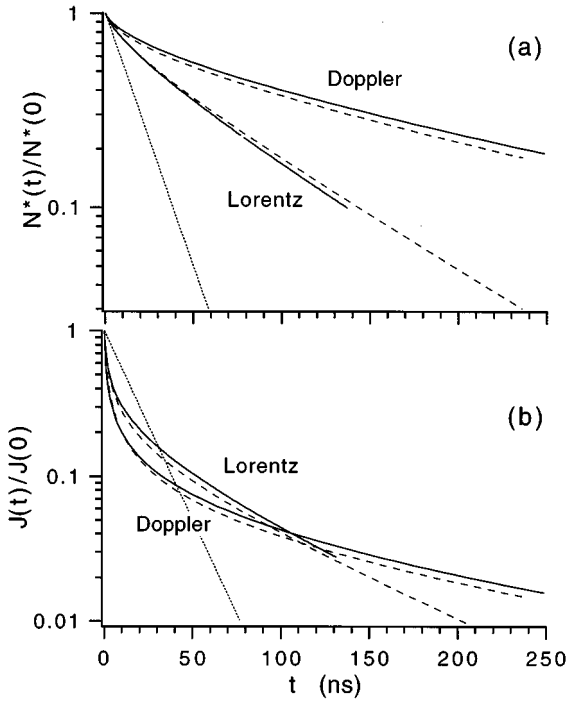

FIG. 6. Entirely excited cylinder with opacity $\tau^{(M)}=10$: normalized decay curves of the total number of excited atoms (a); normalized decay curves of the emerging fluorescence J (b). The solid and dashed lines represent the results of the numerical [12] and analytical [Eqs. (49) and (50)] simulations. The dotted line represent a decay with the natural lifetime.

$$\lambda^2_{\kappa=3}=\frac{3}{8}\ \frac{1-\rho^2/2}{5\rho^3}\ \frac{1+7\rho/3}{1-0.4\rho^2}\Lambda_{\kappa=3}(\tau_A^{(M)}). \qquad (47)$$

The multiplier Λ is determined by Eq. (E2). It reflects the λ-factor dependence on the opacity of region A. The Λ values as a function of the opacity are presented in Fig. 9.

Figures 2–6 demonstrate that our analytical approximations [Eqs. (40)–(47)] provide high accuracy in the evaluation of N_A^* and N_B^* over a large range of variations of both the opacity and laser beam radius $r_A=\rho R$. The accuracy is higher for the slab case (see Figs. 2–4), where we get an accuracy better than 5% for both large and small opacities, over the whole range of ρ values. The error for the cylinder is only slightly worse, but always smaller than 10% (see Figs. 5 and 6). The reason for this is that the geometry correction introduced in Sec. V B is of course not perfect, so that we have an additional source of error (the slab does not need this geometry correction at all). The distribution of excited-state atoms in region B is also accounted for (as far as the reabsorption rate in region A is concerned). The fact that the accuracy for N_B^* is worst of all three considered variables (N^*, N_A^*, N_B^*) is mainly due to the fact that N_B^* is much smaller than N^* at the beginning of the decay, and is computed as the difference $N^*-N_A^*$. Even a comparatively small error in N^*,N_A^* can thus produce a considerable error in N_B^*.

VI. SUBNATURAL FLUORESCENCE DECAY

Basically, there are two ways to observe the decay phenomena in an atomic vapor. One possibility is to send a probe radiation (e.g., radiation tuned to a higher-order resonance transition) into the cell during the decay phase, and observe the absorption of this beam. This provides a measurement for the ground-state density, and allows a direct determination of the parameters that we discussed in the previous subsections. By using an appropriate experimental design, it can even be used to determine the spatial distribution of ground- state (or excited-state) atoms [31]. This requires, however, additional experimental efforts. The other possibility is to observe just the fluorescence radiation J emerging from the vapor cell. There is, of course, a well-defined relation between the excited-state distribution integrated over the whole cell and the emergent radiation: if a photon escapes from the cell, the integrated excited-state density must decrease by one emitting atom. Mathematically, we can formulate this as

$$J\propto-\frac{dN^*}{dt}. \qquad (48)$$

While this relation is well understood and extensively used in linear radiation trapping, the nonlinearity gives rise to some new interesting phenomena that are not clear at first glance, but that can be described by our analytical formulation. It is a common opinion that the radiation trapping leads to an increase of all time scales involved in the decay process, essentially the effective lifetime of the fundamental mode. The nonlinear effects arising from medium bleaching appear to be out of the frame of this description: the emergent radiation can decay with a time constant that is *faster* than the natural lifetime.

This phenomenon, first predicted by numerical simulations in a slab geometry [13], can be explained qualitatively by the role of ''optical shutter'' played by the bleached vapor. The subnatural decay occurs because the photon flux emerging from the cell decreases not only due to the smaller number of excited atoms, but also due to the reabsorption, which increases with time. For the case of a completely excited cell ($\rho=1$), the medium opacity τ at the beginning of the process ($t=0$) is zero. Thus, the photons can escape freely from the cell. During the deexcitation process of n^*, radiation absorption takes place, and photons are trapped by the medium.

As an example, Fig. 6 shows a typical decay curves (numerical simulation, solid curves) of the emergent radiation during excitation of the $3S-3P$ transition of sodium vapors (natural lifetime $\Gamma^{-1}=16.7$ ns) for a cylinder geometry, in the case of entirely excited gas medium ($\rho=1$). Superimposed on the numerical data are theoretical curves obtained for optical opacity $\tau^{(M)}=10$ for both Doppler and Lorentz profiles. The decay of the total excitation N^* shows a behavior that at the beginning decays with the natural lifetime (also shown in Fig. 6 with a dotted line), and later becomes slower. However, the fluorescence intensity $J\propto-dN^*/dt$ exhibits a very fast (subnatural) decay behavior, within a typical time scale well below the natural lifetime, as explained above.

We can describe this effect by explicit analytical formulas [Eqs. (13) and (14), with the corrections of Sec. V]. In Appendix B it is shown that (for $\rho=1$)

$$t\Gamma = I^{(D)}(p) = \frac{2/(1+\Delta)}{\vartheta_{\mathrm{ef},D}^{(m=0.5)}[(\tau^{(M)}/2)(1+\Delta)(1-p)]} \times \left[-\frac{\ln(p)}{1-p} + \frac{\Delta}{2}(1-p) \right], \tag{49}$$

$$t\Gamma = I^{(L)}(p) = \frac{1.5/(\sqrt{1+\Delta})}{\vartheta_{\mathrm{ef},L}^{(m=0.5)}[(\tau^{(M)}/2.25)(1+\Delta)(1-p)]} \frac{1}{\sqrt{1-p}} \times \int_p^1 \frac{du}{u}\sqrt{(1-u)(1+\Delta u)}, \tag{50}$$

where $p = N^*(t)/N^*(t=0)$.

The evaluation of the slope of the J curves provides the local decay rate constant Γ_{ef} for the fluorescence emission:

$$\Gamma_{\mathrm{ef}} = -\frac{1}{J}\frac{dJ}{dt}. \tag{51}$$

According to Eq. (40),

$$\Gamma_{\mathrm{ef}} = -\frac{d\ln N^*}{dt} - \frac{d\ln\vartheta_{\mathrm{ef}}}{dt} = \Gamma\,\vartheta_{\mathrm{ef}}(\tau(t)) - \frac{d}{dt}\ln\vartheta_{\mathrm{ef}}(\tau(t)). \tag{52}$$

For $t\sim 0$, and opacity $\tau\sim 0$, the first term of Eq. (52) gives the natural radiation constant Γ, but the second term, being positive (ϑ_{ef} decreases for increasing τ), tends to increase the Γ_{ef} value.

Experimental confirmation of the subnatural decay has been provided by an experiment involving the $3S\rightarrow 3P$ transition in sodium [16]. Measurements were done in a Pyrex-glass cell shaped as a flat cylinder of height $L=2$ cm, with a diameter $d=5$ cm. The sodium density was $N=1.2\times 10^{12}$ cm^{-3}. This experimental geometry corresponds closely to a slab (see [7,28]) with a total thickness $L=2R=2$ cm. For a Doppler profile this corresponds to an opacity $2\tau^{(M)}=11$.

The whole vessel containing the sodium atoms was excited by a pulsed dye laser tuned to the $3S_{1/2}\rightarrow 3P_{1/2}$ transition at 589.6 nm. Pulse duration was 5 ns full width at half maximum, pulse energy 3 mJ, and the spectral linewidth was about 0.015 nm. For the conditions of the experiment, the line profile was determined only by the Doppler broadening.

The resonance fluorescence light was collected through a flat optical window by an optical fiber and detected by a fast silicon photodiode (rise time <0.3 ns), connected to a fast digital oscilloscope (HP54520A, bandwidth 500 MHz). The fluorescence signal was attenuated by means of neutral density filters in order to prevent detector saturation and ensure its linear response.

The inset of Fig. 7 shows the fluorescence signal (dots) as a function of time for the first 50 ns after the laser shot. The dashed line corresponds to the natural decay curve of the excited sodium level ($\Gamma^{-1}=16.7$ ns). As can be clearly seen in the figure, in the first stage of the process ($t\leqslant 10$ ns) the fluorescence signal displays a decay much faster than the natural one, as predicted by the theory.

Figure 7 shows the fluorescence data recorded in the total decay interval. The solid curves [analytical results obtained using Eq. (49), $\Delta=0$)] show the total photon flux $J=-dN^*/dt$ emerging from the gas medium. Some discrepancies between the experimental data and the theoretical results occur, due to the actual acceptance angle of the optical fiber ($\approx 60°$), which is lower than the 180° angle assumed in the analytical solution. Numerical simulations taking into account the actual detection geometry of the setup have shown an even better agreement with the experimental results, as expected [16].

VII. SUMMARY AND CONCLUSIONS

We have derived an analytical method for the computation of the decay of an atomic vapor excited by a strong short laser pulse. The strong excitation leads to a nonlinearity of the decay process. We derived explicit equations for the excited-state density averaged over the whole cell, and the excited-state density in the initially excited region. The corresponding radiation rate constants (escape factors) were presented in the form of universal analytical expressions, allowing rapid evaluation for arbitrary line profiles. We first derived a very simple approximation that describes the basic features of the process. The accuracy of the method was then increased by introducing correction factors. These correction factors are not some arbitrary numerical fitting factors, but rely on a physically motivated origin, and thus provide an insight into the mechanisms that affect the excited-state density. The equations are valid for all practically important line shapes (Doppler, Lorentz, and Voigt). The accuracy of our analytical formulations was shown to be better than 10% (for Doppler line shapes) by comparing them to numerical solutions; for Lorentz and Voigt line shapes, the accuracy is even better.

The behavior of the excited-state density is affected very strongly by the nonlinearities. The excited-state density decreases much faster than one would expect on the basis of the usual (linear) trapping theory. Most important, the radiation emergent from a cell can decay faster than with the natural lifetime. This fact was confirmed by analytical com-

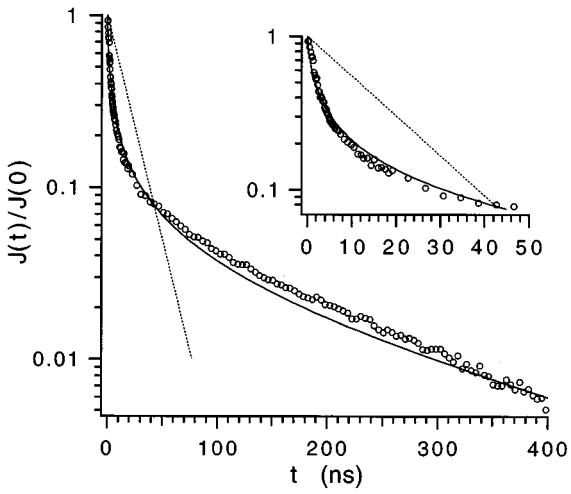

FIG. 7. Normalized decay of the emerging fluorescence: experimental data from Ref. [16] (open circles), analytical results [Eqs. (48) and (49), with $\Delta=0$] obtained for an entirely excited slab with $\rho=1$, decay with the natural lifetime $\Gamma^{-1}=16.7$ ns (dotted line).

putations, numerical simulations, and experiments.

The results and methods presented in this work can be used for the interpretation of experiments where a laser pulse excites a vapor, as, in particular, the investigation of photoresonant plasmas (see [21]). Important parameters of these plasmas, such as the ion density distribution, electron energy distribution function, etc., are strongly related to the excited-state distribution, which we computed in this paper. There is also the possibility to solve, within the frame of the presented method, the inverse problem, i.e., to obtain the radiative and collisional effective rate constants using the integral characteristics of the excited medium. The methods developed in the present work for transferring the results obtained for a plane-parallel slab to a curvilinear geometry can be useful to solve the ionization and radiation trapping phenomena occurring in excited mediums with strongly space-inhomogeneous spectral characteristics, as, for instance, in the spherical geometries typical of aerosol plasmas (see, for example, Ref. [32]).

ACKNOWLEDGMENTS

This work has been supported by NATO Grant No. HTECH.LG 931325. Additional support by PECO-programme Contract No. ERBCIPD CT940633 is also gratefully acknowledged. One of the authors (T.S.) is grateful for Polish Grant No. 57787/DZ/95.

APPENDIX A

In the derivation of Eqs. (18) and (23), we have to analyze first the local escape factor $\vartheta(x)$, which can be suitably expressed as

$$\vartheta(x)=1-\int\int_{-\infty}^{\infty}\int d^3\tilde{x}G(x-\tilde{x})\vartheta_R^{(ch)}(\tilde{x}), \tag{A1}$$

where d^3x indicates the volume integration element dx_1dydz in the (x_1,y,z) space-coordinate system. The characteristic function $\vartheta_R^{(ch)}(\tilde{x})$ restricts the integration in Eq. (A1) over the volume V under investigation. For uniform spatial distribution of ground-state atoms, the kernel $G(x,\tilde{x})$ [see Eq. (4)] depends only on the difference $(x-\tilde{x})$, so that the integral operator in Eq. (A1) is of the convolution type. A convolution operator in the space domain becomes a multiplication operator after Fourier transformation of Eq. (A1):

$$\hat{\vartheta}(p)=[1-\hat{G}(p)]\hat{\vartheta}_R^{(ch)}(p), \tag{A2}$$

$$\hat{G}(p)=\int d^3x\exp(i\vec{p}\cdot\vec{x})G(x)=\int_{-\infty}^{\infty}\frac{\varphi_\nu k_\nu}{|p|}\arctan\left(\frac{|p|}{k_\nu}\right)d\nu, \tag{A3}$$

where $\hat{\vartheta}(p),\hat{G}(p),\hat{\vartheta}_R^{(ch)}(p)$ are the Fourier transforms, in the space of the $p=(p_x,p_y,p_z)$ coordinate, for the corresponding space functions.

The function $\hat{\vartheta}_R^{(ch)}(p)$ is well known [29] to contain a Bessel function $J_{\kappa/2}$ for the geometries here considered:

$$\hat{\vartheta}_R^{(ch)}(p)=(2\pi R)^{\kappa/2}J_{\kappa/2}(|p|R)|p|^{-\kappa/2}\Delta_\kappa(p). \tag{A4}$$

The factor $\Delta_\kappa(p)$ depends on the geometry, being (i) $\Delta_{\kappa=3}(p)=1$ (sphere); (ii) $\Delta_{\kappa=2}(p)=2\pi\delta(p_z)$ (cylinder); (iii) $\Delta_{\kappa=1}(p)=(2\pi)^2\delta(p_x)\delta(p_y)$ (layer).

The inverse Fourier transform for $\hat{\vartheta}(p)$ provides a suitable representation for the local escape factor:

$$\vartheta(r)=\int_0^\infty d|p|\frac{J_{\kappa/2}(|p|R)}{R^{-\kappa/2}}\frac{J_{\kappa/2-1}(|p|r)}{r^{\kappa/2-1}}[1-\hat{G}(|p|)], \tag{A5}$$

which is factorized on the variables R,r. The coordinate r introduced in Eq. (A5) is (i) the distance from the sphere center, for $\kappa=3$; (ii) the radial cylinder coordinate, for $\kappa=2$; (iii) $r=|z|$, that is the distance from the center plane of the layer, for $\kappa=1$.

The rate constants $\vartheta_{\rm ef}^{(m)}$ introduced in Eq. (9) are obtained by averaging $\vartheta(r)$ over r space with a weight function $n_m(r)$ [according to Eq. (9)]:

$$\vartheta_{\rm ef}^{(m)}=\frac{\int_0^R drr^{\kappa-1}\vartheta(r)n_m(r)}{\int_0^R drr^{\kappa-1}n_m(r)}. \tag{A6}$$

Using the identity [29]

$$\int_0^1 drr^{\kappa/2}J_{\kappa/2-1}(pr)(1-r^2)^m=2^m\Gamma(1+m)\frac{J_{\kappa/2+m}(p)}{p^{1+m}}, \tag{A7}$$

the following expression for $\vartheta_{\rm ef}^{(m)}$ is obtained:

$$\vartheta_{\rm ef}^{(m)}=\frac{\Gamma(\kappa/2+m+1)}{\Gamma(\kappa/2)}2^{1+m}\int_0^\infty dpJ_{\kappa/2}(p)\frac{J_{\kappa/2+m}(p)}{p^{1+m}}\times[1-\hat{G}(p/R)]. \tag{A8}$$

The asymptotic expression for $\tau=k_0nR\to\infty$ given in Eq. (18) can then be obtained from Eq. (A8), if the following asymptotic form [5,15,28] is used:

$$1-\hat{G}(p/R)\underset{k_0nR\gg1}{\simeq}\frac{\pi\gamma}{\sin(\pi\gamma)\Gamma(2+2\gamma)}p^{2\gamma}T(k_0nR), \tag{A9}$$

along with the tabulated values for the integral involving two Bessel functions [29].

The integral expression (A8) turns out to be identical to Eq. (23) after insertion of the expression given in Eq. (A3) and some manipulations based on arctan-Bessel functions [29].

APPENDIX B

We shall evaluate here the integral

$$I(p)=\int_p^1\frac{du}{u}\frac{1}{\vartheta_{\rm ef}(\tau^{(M)}(1-u)(1+\Delta u))}, \tag{B1}$$

that is the modification of the integral expressed in Eq. (14) according to the correction given in Eq. (41).

The most straightforward way would be to use the high opacity factorization introduced in Eq. (20) in order to write a factorization for the integral of Eq. (B1):

$$I(p) \underset{\tau^{(M)}\to\infty}{=} \frac{\widetilde{I}(p)}{\vartheta_{ef}(\tau^{(M)})}, \quad \widetilde{I}(p)=\int_p^1 \frac{du}{u}(1-u)^{2\gamma}(1+\Delta u)^{2\gamma}. \tag{B2}$$

However, the above approximation is not valid for $p\sim 1$: the actual behavior of the function $I(p)$ for $p\sim 1$,

$$I(p) \underset{p\to 1}{\simeq} (1-p), \tag{B3}$$

differs strongly from the $\widetilde{I}(p)$ behavior:

$$\widetilde{I}(p) \underset{p\to 1}{\simeq} \frac{(1-p)^{2\gamma+1}}{2\gamma+1}(1+\Delta)^{2\gamma}. \tag{B4}$$

We thus have to find a different factorization of Eq. (B2) that also satisfies the behavior of Eq. (B3). Such a transformation is given by

$$I(p)\simeq \frac{1}{\vartheta_{\rm ef}(\tau^{(M)}(1-p)(1+\Delta)(1+2\gamma)^{-1/2\gamma})}\widetilde{I}(p), \tag{B5}$$

$$\widetilde{I}(p)=\frac{2\gamma+1}{(1+\Delta)^{2\gamma}(1-p)^{2\gamma}}\int_p^1 \frac{du}{u}(1-u)^{2\gamma}(1+\Delta u)^{2\gamma}. \tag{B6}$$

It is straightforward to prove that Eqs. (B5) and (B6) show the factorization of Eq. (B2) for $\tau^{(M)}(1-p)\gg 1$ because of Eq. (20), and lead to Eq. (B3) because all $\vartheta_{\rm ef}^{(m)}(\tau)\sim 1$ for $\tau\sim 0$.

Equations (16) and (49) presented in the text can be derived by explicit integration in Eq. (B6) for $\gamma=0.5$ (Doppler profile); Eq. (15) follows from Eq. (B6) for $\gamma=0.25$, $\Delta=0$ (Lorentz profile). Also in this latter case (Lorentz profile, $\gamma=0.25$) but $\Delta>0$, in fact, the integral in Eq. (B6) [see Eq. (50)] can be expressed as a complicated combination of elementary functions [29]. Equations (15), (16), (49), and (50) turn out to be sufficiently accurate (within a few percent) for all $\tau^{(M)}$,p values and they can be employed for evaluating the integral $I(p)$ within the precision of our approach.

APPENDIX C

As mentioned in Sec. V, we have to analyze two limiting *linear* problems (initial distribution uniform, $\rho=1$, and δ distribution, $\rho=0$) in order to find the correction factors for the one-mode approach. The geometrical quantization technique developed in [30] gives the following expressions for $N^*(t)$ in the Doppler line case:

$$N^*_{\rho=0,1}(t)=f_{0,1}(t)\exp\left(-\frac{t}{\tau_{\rm ef}^{(H)}}\right), \tag{C1}$$

with

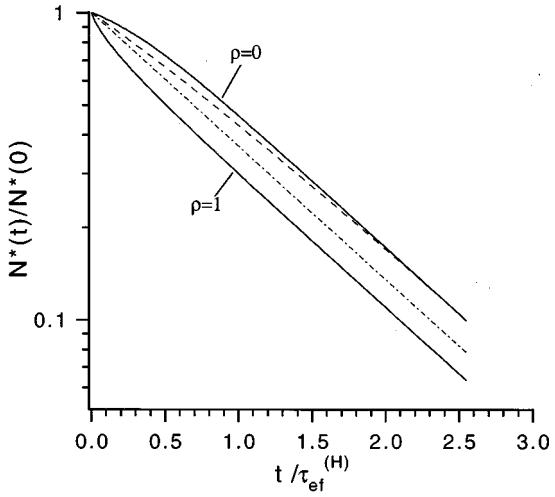

FIG. 8. Normalized decay curves of the total number of excited atoms in an optically thick slab, Doppler line, a weakly excited case. The time t is measured in units of the ground-state Holstein time $\tau_{\rm ef}^{(H)}$. The solid lines represent the exact analytical solutions for $\rho=0$ [Eqs. (C1) and (C2)] and $\rho=1$ [Eqs. (C1) and (C3)], as indicated in the graph; the dashed-dotted line gives the solution obtained with our one-mode approach (both $\rho=0$ and $\rho=1$); the dashed line represents the solution obtained taking into account the correction Eq. (C22) for the case $\rho=0$ as discussed in the text.

$$f_0(t)=\frac{4}{\pi}\exp(a\widetilde{t})\arctan[\exp(-a\widetilde{t})], \tag{C2}$$

$$f_1(t)=\frac{8}{\pi^2}\exp(a\widetilde{t})\int_0^{\exp(-a\widetilde{t})}\frac{dy}{2y}\ln\left(\frac{1+y}{1-y}\right), \tag{C3}$$

$$a=\frac{4}{3}+\frac{11}{12}\frac{\ln(\frac{11}{6})}{\ln(2\tau)}, \qquad \widetilde{t}=\frac{t}{\tau_{\rm ef}^{(H)}}. \tag{C4}$$

Both $N^*_{\rho=0,1}$ $(t=0)$ values are normalized to unity, and the time $\widetilde{t}$ is measured in units of the effective lifetime of the fundamental mode $\tau_{\rm ef}^{(H)}=1/(\Gamma g_f)$ (Doppler profile). The temporal behavior of both $N^*_{\rho=0,1}$ is shown in Fig. 8 (solid curves); this result is equivalent to taking into account all modes with their respective decay time constants. The one-mode approach (Fig. 8, dashed-dotted curve), i.e., Eq. (8) with the assumption of $m=0.5$ for all times, is equivalent to ignoring all the higher-order modes (we neglect here the difference between the lowest-order mode decay factor $g_f=\vartheta_{\rm ef}^H$ and $\vartheta_{\rm ef}^{(m=0.5)}$ values).

As can be seen in Fig. 8, the functions $f_{0,1}$ in Eq. (C1) have a monotonic behavior from $f_{0,1}(t=0)=1$ to

$$f_{\rho=0,1}(t) \underset{t\to\infty}{\simeq} c, \tag{C5}$$

with

$$c^{(D)}_{\rho=0}=\frac{4}{\pi}\simeq 1.27, \tag{C6}$$

$$c^{(D)}_{\rho=1}=\frac{8}{\pi^2}\simeq 0.81. \tag{C7}$$

For the initial δ distribution, the fact that c is larger than unity can be interpreted in the following way: at early times, fewer photons can escape (because the emitting atoms are concentrated in the center of the medium). The fact is also reflected in a larger total density at late times; i.e., the *amplitude* of the lowest-order mode is larger. For the uniform initial distribution, the explanation is the other way round.

We have thus derived the error at late times for the special case of an initial δ distribution and an initial uniform distribution. For the more general case of initial function $n_\rho^*(x,t=0)=n_\rho^*(r)$ with $0<\rho<1$, the results can be obtained from the usual Fourier (multi mode) theory. In this case, the excited-state distribution is given by

$$n_\rho^*(t,x)=\sum_{l=0}^{\infty}\langle n_\rho^*|\psi_l\rangle\langle\psi_l|x\rangle\exp(-\Gamma g_l t), \tag{C8}$$

where, according to Dirac notations, $\langle\psi_l|x\rangle=\psi_l(x)$ is the normalized space distribution for the l mode, g_l is the corresponding escape factor, and $\langle f|\tilde{f}\rangle$ indicates the scalar product:

$$\langle f|\tilde{f}\rangle=\int_0^R \frac{dr r^{\kappa-1}}{R^\kappa/\kappa} f(r)\tilde{f}(r). \tag{C9}$$

Function $n_\rho^*(r)$ is of the space-step type: $n_\rho^*=1$ when $r<\rho$ and $n_\rho^*=0$ for $r>\rho$.

In the one-mode decay regime, for $t\to\infty$ all terms in Eq. (C8), except those referring to the fundamental mode ($l=0$), vanish. Thus, for $N^*(t)$ we have

$$N^*(t)\equiv\langle n_\rho^*(t)|n_{m=0}\rangle \underset{t\to\infty}{=} \langle n_\rho^*|\psi_f\rangle\langle\psi_f|n_{m=0}\rangle\exp(-\Gamma g_f t)$$

$$=c_0\exp(-\Gamma g_f t), \tag{C10}$$

where $n_{m=0}(x)$ denotes the uniform function $n_{m=0}(x)=1$ in the volume V, and ψ_f is the normalized ground-state mode. An approximate expression of ψ_f is [see Eq. (12)]

$$\psi_f=A_0\left(1-\frac{r^2}{R^2}\right)^\gamma, \tag{C11}$$

$$A_0^2=\frac{\Gamma(\kappa/2+2\gamma+1)}{\Gamma(\kappa/2+1)\Gamma(2\gamma+1)}, \tag{C12}$$

where the constant A_0 is the normalization factor for the space weight function $r^{\kappa-1}/(R^\kappa/\kappa)$ appearing in Eq. (C9).

According to our approach [see Eq. (11)], the temporal behavior $N^*_{\rm app}$ with the initial condition $N^*(t=0)=\langle n_\rho^*|n_{m=0}\rangle$ is

$$N^*_{\rm app}(t)=\tilde{c}_0\exp(-\Gamma g_f t), \tag{C13}$$

with $\tilde{c}_0=\langle n_\rho^*|n_{m=0}\rangle$. The ratio $c=c_0/\tilde{c}_0$ plays the same role (late-time deviation from the case that the initial distribution is the fundamental mode) as that of the constant c in the decay of Eq. (C5). The decrease of c from the initial ($t=0$) unit value is a measure of the inaccuracy of the one-mode approach. Using Eqs. (C10) and (C13), we obtain for c:

$$c=\frac{\Gamma(\kappa/2+2\gamma+1)\Gamma(\gamma+1)}{\Gamma(2\gamma+1)\Gamma(\kappa/2+\gamma+1)}F(-\gamma,\kappa/2;1+\kappa/2,\rho^2), \tag{C14}$$

where F is the hypergeometrical function [29].

The expression Eq. (C14) can be simplified by using the series expansion of the function F [29] for the two limit cases $\rho\simeq 0$ and $\rho\simeq 1$:

$$c=\frac{\Gamma(\kappa/2+2\gamma+1)\Gamma(\gamma+1)}{\Gamma(2\gamma+1)\Gamma(\kappa/2+\gamma+1)}, \quad \rho\simeq 0, \tag{C15}$$

$$c=\frac{\Gamma(\kappa/2+2\gamma+1)\Gamma^2(\gamma+1)\Gamma(\kappa/2+1)}{\Gamma(2\gamma+1)\Gamma^2(\kappa/2+\gamma+1)}\frac{1}{\rho^\kappa}, \quad \rho\simeq 1. \tag{C16}$$

Table II gives the values of the c factor (in brackets for Doppler profile), evaluated according to Eqs. (C15) and (C16) for the geometries and the spectral profiles investigated in this paper.

The difference ($\simeq 10\%$) between the c values appearing in Eqs. (C6) and (C7) and those reported in Table II in brackets (for slab, Doppler case, $\rho=0$, $\rho=1$) are caused by the fact that the spatial distribution of the fundamental mode is not exactly identical to the power-law distribution with $m=0.5$. This fact produces some error in the evaluation of the overlapped integrals $\langle\psi_f|n_\rho^*\rangle$ and $\langle\psi_f|n_{m=0}\rangle$ entering the ratio $c_0/\tilde{c}_0$. Note that, when exploiting the variational method for the evaluation of the g_f factor for the fundamental mode, overlapped integrals $\langle\psi_0|f\rangle$ of the same kind are encountered. Thus, the occurrence of a similar discrepancy ($\simeq 10\%$) between the factors $\vartheta_{\rm ef}^{(m=0.5)}$ and g_f (see Table I) is not surprising. As these discrepancies are observed also for the cylinder and sphere geometries (Doppler case, see Table I), in order to reduce the problems related to the one-mode approach for the Doppler case, we have to increase the c values (in brackets, Table II) from the declared unit value by a factor 10%, as reported in Table II. On the contrary, for the Lorentz profile the $\vartheta_{\rm ef}^{(m=0.5)}$ and g_f are almost identical, since the escape factor depends much less on the spatial distribution of the excited atoms, so no correction to the c values is required.

The above error analysis also forms the basis for the introduction of a correction factor. Let us consider the case $\rho=0$. At early times, we have to increase the optical opacity by a factor Δ [$\tau^{(M)}\to\tau^{(M)}(1+\Delta)$] in order to change the steepness of the decay curve (see Fig. 8, solid curve), i.e., in order to recover the behavior computed above. At late times, this Δ correction must vanish. At intermediate times, we need some kind of interpolation. The easiest way to include such a time-varying correction is to take $\Delta=\Delta_\rho N^*(t)/[N^*(t=0)]$. This leads, in Eq. (11), to the replacement:

$$\tau^{(M)}\to\tau^{(M)}\left(1+\Delta_\rho\frac{N^*(t)}{N^*(t=0)}\right). \tag{C17}$$

The corresponding solution,

$$t\Gamma=\int_{N^*(t)/N^*(t=0)}^{1}\frac{du}{u\,\vartheta_{ef}^{(m=0.5)}(\tau^{(M)}(1+\Delta_\rho u))}, \quad \text{(C18)}$$

is obtained for $\rho\sim 0$, when $V_A/V\sim\rho^\kappa\sim 0$. For large Doppler opacities ($\tau^{(M)}\gg 1$), the factorization $1/\vartheta_{\rm ef}(\tau^{(M)}(1+\Delta_\rho u))=(1+\Delta_\rho u)/\vartheta_{\rm ef}(\tau^{(M)})$ can be introduced [see Eq. (20)], which allows to write Eq. (C18) as

$$t\Gamma\,\vartheta_{\rm ef}^{(m=0.5)}(\tau^{(M)})=-\ln\left(\frac{N^*(t)}{N^*(t=0)}\right)+\left(1-\frac{N^*}{N^*(t=0)}\right)\Delta_\rho. \quad \text{(C19)}$$

For $N^*(t)\ll N^*(t=0)$ (one-mode regime) it is

$$\frac{N^*}{N^*(t=0)}_{t\to\infty}=\exp\left(-\frac{t}{\tau_{\rm ef}^{(H)}}\right)\exp(\Delta_\rho). \quad \text{(C20)}$$

Equation (C20) is identical to the exact solution [Eqs. (C1) and (C5)] for $t\to\infty$, if we make the following substitution

$$\exp(\Delta_\rho)\simeq 1+\Delta_\rho=c. \quad \text{(C21)}$$

The dashed curve of Fig. 8 has been obtained by using Eq. (C19) for $\Delta_{\rho=0}^{(D)}=c_{\rho=0}^{(D)}-1=\pi/4-1$. It demonstrates the considerable improvement of the accuracy (to better than 5%) achieved by including the modifications of Eq. (C17) in the solution of the master rate equation [Eq. (11)].

For the case $\rho>0$, the corrections are smaller due to the nonlinear effects mentioned in Sec. V A. Moreover, in the case $\rho=1$, the bleaching of the vapor at early times causes the $(c_{\rho=1}-1)$ value to be practically zero (see the discussion in Sec. V A). Thus, the Δ_ρ variation on ρ from the initial value $\Delta_{\rho=1}=0$ to $\Delta_{\rho=0}=c_{\rho=0}-1$ can be approximated as

$$\Delta_\rho=(1-\rho^\kappa)(c_{\rho=0}-1) \quad . \quad \text{(C22)}$$

The appearance of the κ power in Eq. (C22) is caused by the fact that the same power index appears in Eqs. (C15) and (C16) for the c factors.

APPENDIX D

The considered geometrical model for a partly excited cylinder or sphere at the beginning of the decay is a cylinder (or a sphere) with a hole inside (simulating the region without absorption), filled with emitting atoms [see Fig. 1(d)]. We investigate here in detail the case $\rho\sim 1$. Photon absorption occurs at the cylinder (or sphere) boundary S, in a layer with a small thickness, $R-r_A\ll R$, but with a rather large optical opacity, $\tau=k_0 n(R-r_A)\gg 1$.

Since the geometrical dimension of the absorbing region $(R-r_A)$ is small compared to R, we can approximate the optical path $k_0 n\Delta L$ traveled by the photon emitted at distance r from the cell center [see Fig. 1(d)] as

$$k_0 n\Delta L=\frac{\tau}{\cos\phi_r}. \quad \text{(D1)}$$

Here, the angle ϕ_r lies in front of the side r in the triangle OrR [see Fig. 1(d)]. For a cylinder, $\vartheta(r)$ is defined as

$$\vartheta_C(r)=\int_{\phi,\theta}\frac{d\Omega}{4\pi}\int d\nu\,\varphi_\nu\exp\left(-\theta_\nu\frac{\tau}{\sin\theta\cos\phi_r}\right), \quad \text{(D2)}$$

where ϕ,θ are the angles determining the photon flight direction in a spherical coordinate system centered in r, and $d\Omega=\sin\theta d\theta d\phi$ is the solid angle. For a sphere, the expression for ϑ is similar, but in this case the term $\sin\theta$ must be dropped.

The inner integral (integration over the frequency variable ν) gives a transmission factor T [Eq. (19)] (for the path determined by θ and ϕ). Using the factorization properties of T [Eq. (20)], we can write Eq. (D2) as

$$\vartheta_C(r)=T(\tau)\int_0^\pi\frac{d\theta}{2}(\sin\theta)^{2\gamma+1}\int_0^{2\pi}\frac{d\phi}{2\pi}\cos^{2\gamma}(\phi_r), \quad \text{(D3)}$$

with the properties

$$R\sin\phi_r=r\sin\phi, \quad \cos^2(\phi_r)=1-\frac{r^2}{R^2}\sin^2\phi, \quad \text{(D4)}$$

where the notations of Fig. 1(d) have been used.

Two limiting cases can be evaluated easily: emission in the center of the hollow cylinder (i.e., $r=0$) and emission close to the boundary S ($r\simeq R$). In the former case, $\phi_r=0$, while in the latter, $\phi_r=\phi$. With these simplifications, Eq. (D3) reduces to

$$\vartheta_C(r=0)=T(\tau)\frac{\sqrt{\pi}\Gamma(1+\gamma)}{2\Gamma(\gamma+1.5)},$$

$$\vartheta_C(r=R)=T(\tau)\frac{1}{1+2\gamma}. \quad \text{(D5)}$$

When we compare these expressions to Eq. (18) with $m=\infty$ (δ localization of the distribution, the expression in brackets being equal to unity), we see that $\vartheta_C(r=0)$ as given in Eq. (D5), is identical to $\vartheta_{\rm ef}^{(\delta)}(\tau)$ for $\kappa=2$ (cylinder). Similarly, $\vartheta_C(r=R)$ is identical to $\vartheta_{\rm ef}^{(\delta)}(\tau)$ for $\kappa=1$ (slab). This can also be interpreted physically: a hollow cylinder as seen from its center is a normal cylinder with optical thickness τ; a photon emitted close to the boundary, on the other hand, ''sees'' a plane-parallel layer.

The escape factor ϑ_ρ for $\rho\sim 1$, determining the total photon flux, is an average of $\vartheta(r)$ over the cylinder (or sphere) volume:

$$\vartheta_\rho(\tau)=\int_0^R\frac{dr r^{\kappa-1}}{R^\kappa/\kappa}\vartheta(r). \quad \text{(D6)}$$

The integration over r can be performed analytically for $\vartheta(r)$ [Eq. (D3)], exploiting the properties given in Eq. (D4). The final results for both cylinder (C) and sphere (S) are

$$\vartheta_{\rho\simeq 1}^{(C)}=\frac{2}{\sqrt{\pi}}\frac{\Gamma(\gamma+1.5)}{\Gamma(\gamma+2)}\vartheta_{{\rm ef},\kappa=2}^{(\delta)}(\tau), \quad \text{(D7)}$$

$$\vartheta_{\rho\simeq 1}^{(S)}=\frac{1}{1+2\gamma/3}\vartheta_{{\rm ef},\kappa=3}^{(\delta)}(\tau), \quad \text{(D8)}$$

where the subscript κ indicates the geometry according to the notations introduced for Eq. (18).

With the factorization of Eq. (20), we can rewrite Eq. (D7) in such a way that we have a correction in the *argument* of the escape factor.

For a sphere, we use the approximation $(1+2\gamma/3) \approx (1+1/3)^{2\gamma}$, to get

$$\vartheta_{\rho=1}^{(S)} \simeq \vartheta_{\mathrm{ef},\kappa=3}^{(\delta)}((1+\Delta)\tau), \quad \Delta_S = \tfrac{1}{3}. \tag{D9}$$

For a cylinder, this procedure is more complicated. Let us introduce the function $f(\gamma) = \sqrt{\pi}\,\Gamma(\gamma+2)/[2\Gamma(\gamma+1.5)]$. A series expansion over γ for such function gives, for the first terms, $f(\gamma) \simeq 1+[(\ln 4-1)/2]2\gamma \simeq [1+(\ln 4-1)/2]^{2\gamma}$. Including this series expansion into Eq. (D7), we get

$$\vartheta_{\rho}^{(C)} = \vartheta_{\mathrm{ef},\kappa=2}^{(\delta)}((1+\Delta)\tau), \quad \Delta_C = \frac{\ln 4-1}{2} \simeq 0.19. \tag{D10}$$

APPENDIX E

The factor λ mentioned in Sec. V C can be computed from the requirement that the behavior at late times should be correct. Let us thus rewrite the rate equation (42) for the final stage of the decay, ruled by the fundamental mode characteristics when $N_i^*(t) \sim N_i^* \exp(-\Gamma g_f t)$:

$$-g_f(\tau^{(M)})N_A^* = -g_f(\tau_A^{(M)})N_A^* + (N^*-N_A^*)\frac{1}{\lambda}\vartheta_{\mathrm{ex}}(\tau_A^{(M)}\lambda). \tag{E1}$$

It is worth while to recall that we make no difference between the escape factors g_f and $\vartheta_{\mathrm{ef}}^{(m=0.5)}$. Thus, Eq. (E1) allows a straightforward determination of the λ values:

$$\lambda^{1+2\gamma}(1-\rho^{2\gamma}) = \frac{N-N_A^*}{N_A^*}\frac{\vartheta_{\mathrm{ex}}(\infty)}{g_f(\infty)}\Lambda(\tau_A^{(M)}),$$

$$\Lambda(\tau_A^{(M)}) = \frac{\vartheta_{\mathrm{ex}}(\tau_A^{(M)})}{g_f(\tau_A^{(M)})}\frac{g_f(\infty)}{\vartheta_{\mathrm{ex}}(\infty)}, \tag{E2}$$

by using the factorization expressed in Eq. (20) for large $\tau^{(M)}$, $\tau_A^{(M)}$:

$$\frac{g_f(\tau^{(M)})}{g_f(\tau_A^{(M)})} = \left(\frac{\tau_A}{\tau}\right)^{2\gamma} = \rho^{2\gamma},$$

$$\vartheta_{\mathrm{ex}}(\lambda\tau_A)\lambda^{-1} = \vartheta_{\mathrm{ex}}(\tau_A)\lambda^{-1-2\gamma}. \tag{E3}$$

We have introduced into Eq. (E2) a variable Λ depending on the region A optical opacity. For the sake of simplicity, a special normalization $\Lambda(\tau_A^{(M)}=\infty)=1$ is chosen for all geometries under consideration (see Fig. 9). Note that, from the asymptotic behavior of $\vartheta_{\mathrm{ex}}(\tau)$ [see Eq. (34)], it follows $\vartheta_{\mathrm{ex}}/g_f = (2\gamma)\vartheta_{\mathrm{ef}}^{(\delta)}/(\kappa g_f)$ for large τ.

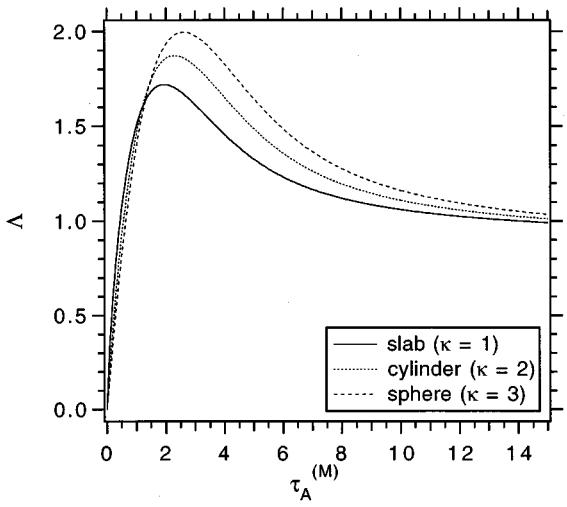

FIG. 9. Dependence of Λ determined by Eq. (E2) on the the optical opacity $\tau_A^{(M)}$ of region A. All curves are normalized to the unit value at the infinity ($\tau_A^{(M)} \to \infty$) for three geometries: (i) a sphere—$\kappa=3$ (dashed); (ii) a cylinder—$\kappa=2$ (dotted); (iii) a slab— $\kappa=1$ (solid).

According to the considerations presented above, the analysis of Eq. (E1) for the Doppler profile case $\gamma_D = 0.5$ is the most important. The approximation given in Eq. (12) allows one to write explicitly the values of N^* and N_A^* involved in Eq. (E1):

$$N^* = \int_0^R dr r^{\kappa-1}\sqrt{1-\frac{r^2}{R^2}}, \quad N_A^* = \int_0^{\rho R} dr r^{\kappa-1}\sqrt{1-\frac{r^2}{R^2}}. \tag{E4}$$

The final result, which can be obtained by exploiting the ratio $\vartheta^{(\delta)}/g_f$ reported in Table I, and performing some manipulations, gives expressions of λ for the three geometries under investigation:

$$\lambda_{\kappa=1}^2 = \frac{\pi}{4}\ \frac{1-\rho^2/2}{2\rho}\ \frac{1-\rho[1-8/(3\pi)]}{1-\rho^2(1-\pi/4)}\Lambda_{\kappa=1}(\tau_A^{(M)}), \tag{E5}$$

$$\lambda_{\kappa=2}^2 = \frac{4}{3\pi}\ \frac{1-\rho^2/2}{3\rho^2}\ \frac{1+\rho}{1-\rho^2/3}\Lambda_{\kappa=2}(\tau_A^{(M)}), \tag{E6}$$

$$\lambda_{\kappa=3}^2 = \frac{3}{8}\ \frac{1-\rho^2/2}{5\rho^3}\ \frac{1+7\rho/3}{1-0.4\rho^2}\Lambda_{\kappa=3}(\tau_A^{(M)}). \tag{E7}$$

Speaking strictly, in Eqs. (E5), (E6), and (E7), the term $\sqrt{1-\rho^2}$ has to be stand instead of the multiplier $(1-\rho^2/2)$. It means that $\lambda \sim 0$ when $\rho \sim 1$; i.e., we have no correction factor due to region B, if region B does not exist. However, if the factor λ has zero value, the second equality of Eq. (E3) fails to be valid. For this reason we have replaced $\sqrt{1-\rho^2}$ by its expansion $(1-\rho^2/2)$.

This substitution does not affect noticeably our results for

$\rho<0.8$. On the other hand, for $\rho>0.8$ the region B cannot influence strongly the zone-A excitation, so that the exact value of λ turns out to be of secondary importance.

It is interesting to note that when $\tau_A>1$ and $1\gg\rho$ the correction factor λ is larger than unity indeed. This fact leads to a decrease of the rate constant ϑ_{ex} for secondary reabsorption in region A that is physically reasonable as it was discussed above: if all emitting atoms are assumed to be near region A (i.e., without correction), then, of course, also the reabsorption rate is higher than when the emitting atoms are distributed all over the region B (which can have a large size).

[1] A. G. Mitchell and M. W. Zemanski, *Resonance Radiation and Excited Atoms* (Cambridge University Press, Cambridge, 1961).

[2] A. Corney, *Atomic and Laser Spectroscopy* (Oxford University Press, Oxford, 1977).

[3] T. Holstein, Phys. Rev. **72**, 1212 (1947); **83**, 1159 (1951).

[4] L. M. Biberman, Zh. Éksp. Teor. Fiz. **17**, 416 (1947).

[5] C. van Trigt, Phys. Rev. **181**, 97 (1969); Phys. Rev. A **1**, 1298 (1970); **4**, 1303 (1971); **13**, 726 (1976).

[6] H. A. Post, Phys. Rev. A **33**, 2003 (1986).

[7] A. F. Molisch, B. P. Oehry, and G. Magerl, J. Quant. Spectrosc. Radiat. Transfer **48**, 377 (1992).

[8] D. Mihalas, *Stellar Atmospheres*, 2nd ed. (Freeman, San Francisco, 1978).

[9] A. E. Bulishev, V. I. Denisov, N. G. Preobrazhenskii, and A. E. Suvorov, Opt. Spectrosc. **59**, 419 (1985).

[10] E. D. Brooks III, and J. A. Fleck Jr., J. Comput. Phys. **67**, 59 (1986).

[11] J. P. Apruzese, Phys. Rev. E **47**, 2798 (1993).

[12] A. F. Molisch, B. P. Oehry, W. Schupita, and G. Magerl, Opt. Commun. **118**, 520 (1995).

[13] T. Stacewicz, T. Kotowsky, P. Wievior, and J. Chorazy, Opt. Commun. **100**, 99 (1993).

[14] N. N. Bezuglov, A. N. Klucharev, B. B. Taratin, T. Stacewicz, A. F. Molisch, F. Fuso, and M. Allegrini, Opt. Commun. **120**, 249 (1995).

[15] V. V. Ivanov, *Transfer of Radiation in Spectral Lines*, NBS Special Publication No. 385 (U.S. GPO, Washington, DC, 1973).

[16] J. Chorazy, T. Kotowski, and T. Stacewicz, Opt. Commun. **125**, 65 (1996).

[17] R. M. Measures and P. G. Cardinal, Phys. Rev. A **23**, 804 (1981).

[18] N. B. Delone, and V. P. Krainov, *Atoms in a Strong Light Field* (Moscow Press, Moscow, 1978).

[19] T. B. Lucatorto and T. J. Mc Iltrath, Phys. Rev. Lett. **37**, 428 (1976).

[20] T. Stacewicz and W. Latek, Phys. Scr. **42**, 658 (1990).

[21] N. N. Bezuglov, A. N. Klucharev, and T. Stacewicz, Opt. Spectrosc. **77**, 301 (1994) [Opt. Spektrosk. **77**, 342 (1994)].

[22] L. M. Biberman, V. S. Vorobjev, and I. T. Yakubov, *Kinetics of Nonequilibrium Low-Temperature Plasma* (Moscow, 1982; Plenum Publ. Corp., New York, 1987).

[23] F. E. Irons, J. Quantum Spectrosc. Radiat. Transfer **22**, 1 (1979); **22**, 21 (1979); **22**, 37 (1979).

[24] N. N. Bezuglov and Y. B. Golubovskij, Opt. Spectrosc. **50**, 122 (1981) [Opt. Spektrosk. **50**, 231 (1981)].

[25] E. B. Aleksandrov and N. N. Jiakobson, Usp. Fiz. Nauk **131**, 721 (1980) [Sov Phys. Usp. **23**, 520 (1980)].

[26] A. F. Molisch, M. Allegrini, B. P. Oehry, W. Schupita, and G. Magerl, Opt. Commun. **120**, 149 (1995).

[27] J. Huennekens and A. Gallagher, Phys. Rev. A **28**, 238 (1983).

[28] A. N. Klucharev and N. N. Bezuglov, *Processes of Excitation and Ionization of Atoms During Light Absorption* (Leningrad State University Press, Leningrad, 1983).

[29] I. S. Gradstein and I. M. Ryzhik, *Tables of Series, Products and Integrals* (Academic, New York, 1994).

[30] R. I. Asadullina, N. N. Bezuglov, and E. N. Borisov, Opt. Spectrosc. **67**, 209 (1989) [Opt. Spektrosk. **67**, 360 (1989)].

[31] W. Molander, M. Belsley, A. Streater, and K. Burnett, Phys. Rev. A **29**, 1548 (1984).

[32] R. I. Asadullina, N. N. Bezuglov, A. N Klucharev, and V. Yu. Sepman, Opt. Spectrosc. **76**, 509 (1994) [Opt. Spektrosk. **76**, 569 (1994)].